

Influences of Biofriendly Amino Acids on Methane Hydrate
Formation for Natural Gas Storage and Transportation
Application



A Thesis Submitted in Partial Fulfillment of the Requirements
for the Degree of Master of Science in Petrochemical Technology
Common Course
the Petroleum and Petrochemical College
Chulalongkorn University
Academic Year 2021
Copyright of Chulalongkorn University

ผลของกรดอะมิโนต่อการเกิดมีเทนไฮเดรต สำหรับการประยุกต์ใช้ในการกักเก็บและการขนส่ง
แก๊สธรรมชาติ



วิทยานิพนธ์นี้เป็นส่วนหนึ่งของการศึกษาตามหลักสูตรปริญญาวิทยาศาสตรมหาบัณฑิต
สาขาวิชาเทคโนโลยีปิโตรเคมี ไม่สังกัดภาควิชา/เทียบเท่า
วิทยาลัยปิโตรเลียมและปิโตรเคมี จุฬาลงกรณ์มหาวิทยาลัย
ปีการศึกษา 2564
ลิขสิทธิ์ของจุฬาลงกรณ์มหาวิทยาลัย

Thesis Title	Influences of Biofriendly Amino Acids on Methane Hydrate Formation for Natural Gas Storage and Transportation Application
By	Mr. Chuvich Chaovarin
Field of Study	Petrochemical Technology
Thesis Advisor	Professor PRAMOCH RANGSUNVIGIT, Ph.D.
Thesis Co Advisor	Santi Kulprathipanja, Ph.D.

Accepted by the the Petroleum and Petrochemical College, Chulalongkorn University in Partial Fulfillment of the Requirement for the Master of Science

..... Dean of the the Petroleum and Petrochemical College
(Professor PRAMOCH RANGSUNVIGIT, Ph.D.)

THESIS COMMITTEE

..... Chairman
(Professor APANEE LUENGNARUEMITCHAI, Ph.D.)
..... Thesis Advisor
(Professor PRAMOCH RANGSUNVIGIT, Ph.D.)
..... Thesis Co-Advisor
(Santi Kulprathipanja, Ph.D.)
..... External Examiner
(Tanate Danuthai, Ph.D.)

จุฬาลงกรณ์มหาวิทยาลัย
CHULALONGKORN UNIVERSITY

ชิวิช เชาวรินทร์ : ผลของกรดอะมิโนต่อการเกิดมีเทนไฮเดรต สำหรับการประยุกต์ใช้ในการกักเก็บและการขนส่ง
 แก๊สธรรมชาติ. (Influences of Biofriendly Amino Acids on Methane Hydrate
 Formation for Natural Gas Storage and Transportation Application) อ.ที่
 ปริญญาหลัก : ศ. ดร.ปราโมช รังสรรค์วิจิตร, อ.ที่ปรึกษาร่วม : ดร.สันติ กุลประทีปปัญญา

การกักเก็บแก๊สในรูปของแข็ง (Solidified natural gas) เป็นการกักเก็บแก๊สธรรมชาติในรูปของคลาเทรตไฮเดรต อย่างไรก็ตามในกระบวนการสร้างนั้นมีอัตราการก่อตัวของไฮเดรตช้าและต้องอยู่ที่สภาวะความดันสูงและอุณหภูมิต่ำเพื่อลดข้อจำกัดดังกล่าว การเติมตัวเร่งการเกิดแก๊สไฮเดรต (Hydrate promoter) เช่น สารลดแรงตึงผิวและกรดอะมิโน เพื่อเพิ่มอัตราการก่อตัวของไฮเดรต มีรายงานว่ากรดอะมิโนมีประสิทธิภาพในการใช้เป็นตัวเร่งการสร้างไฮเดรต นอกจากนี้การเพิ่มการถ่ายโอนมวลด้วยการออกแบบเครื่องปฏิกรณ์ใหม่ ถือเป็นอีกวิธีในการปรับปรุงกระบวนการสร้างไฮเดรต ดังนั้นในงานวิจัยนี้ศึกษาผลของการเติมกรดอะมิโนที่มีโครงสร้างแตกต่างกัน 3 ชนิด ได้แก่ เมทไธโอนีน ลิวซีน และ วาลีน ต่อการสร้างและการแยกตัวของมีเทนไฮเดรตในด้านจลนศาสตร์และสัณฐานวิทยา โดยทำการศึกษาที่สภาวะความดัน 8 เมกะปาสกาล และ อุณหภูมิ 277.2 เคลวิน ในระบบการกวนแบบไฮบริด ที่ความเข้มข้นของกรดอะมิโนในช่วง 0.10-1.00 % โดยน้ำหนัก ผลการศึกษาแสดงให้เห็นว่ากรดอะมิโนช่วยลดเวลาในการเหนี่ยวนำและเพิ่มอัตราการสร้างมีเทนไฮเดรต โดยเฉพาะเมทไธโอนีน กรดอะมิโนดังกล่าวจะส่งผลชัดเจนยิ่งขึ้นเมื่อเพิ่มความเข้มข้น อย่างไรก็ตามกรดอะมิโนไม่ส่งผลต่อปริมาณแก๊สมีเทนที่ถูกจัดเก็บเมื่อสิ้นสุดกระบวนการและปริมาณการเปลี่ยนน้ำเป็นไฮเดรตในทุกการทดลอง นอกจากนี้รูปแบบการสร้างมีเทนไฮเดรตมีลักษณะที่คล้ายคลึงกันในทุกการทดลอง ในกระบวนการแยกตัวของไฮเดรต แก๊สมีเทนที่ได้กลับคืนมามีค่าสูงกว่า 95 % และไม่เกิดโฟมระหว่างกระบวนการแยกตัวของไฮเดรต

จุฬาลงกรณ์มหาวิทยาลัย
 CHULALONGKORN UNIVERSITY

สาขาวิชา เทคโนโลยีปิโตรเคมี
 ปีการศึกษา 2564

ลายมือชื่อนิสิต
 ลายมือชื่อ อ.ที่ปรึกษาหลัก
 ลายมือชื่อ อ.ที่ปรึกษาร่วม

6371002563 : MAJOR PETROCHEMICAL TECHNOLOGY

KEYWORD Solidified natural gas/ Gas hydrates/ Hydrate promoters/ Amino
D: acids/ Clathrate hydrates

Chuvich Chaovarin : Influences of Biofriendly Amino Acids on Methane Hydrate Formation for Natural Gas Storage and Transportation Application. Advisor: Prof. PRAMOCH RANGSUNVIGIT, Ph.D. Co-advisor: Santi Kulprathipanja, Ph.D.

Solidified natural gas (SNG) is an appealing option for storing natural gas in the form of clathrate hydrates. However, it has some limitations, particularly the slow rate of hydrate formation and the requirement for severe operating conditions. To overcome these constraints, one approach is to introduce promoters into the system to enhance the hydrate formation rate. Amino acids have been reported as kinetic promoters with the potential to improve methane hydrate formation. In this work, the effect of three different side-chain amino acids (L-methionine, L-leucine, and L-valine) on methane hydrate formation and dissociation was investigated in terms of kinetics and morphology. The experiments were conducted at 8 MPa and 277.2 K using a hybrid combinatorial reactor approach at various amino acid concentrations (0.1 to 1.0 wt%). Results showed that the presence of amino acids significantly decreased the induction time and increased the rate of methane hydrate formation. In addition, L-methionine was shown to be the most effective kinetic promoter in this work. However, the final methane uptake and the water to hydrate conversion were the same in all experiments. For all investigated experiments, the morphology of methane hydrate formation exhibited a similar pattern, including methane bubbles and capillary channels. In terms of hydrate dissociation, methane recovery was greater than 95% in all studies, and no foam was generated during dissociation, which is favorable for large-scale applications.

จุฬาลงกรณ์มหาวิทยาลัย
CHULALONGKORN UNIVERSITY

Field of Study:	Petrochemical Technology	Student's Signature
	
Academic	2021	Advisor's Signature
Year:	
		Co-advisor's Signature
	

ACKNOWLEDGEMENTS

First and foremost, I would like to express the deepest gratitude to my advisor, Prof. Pramoch Rangsunvigit, and co-advisor, Dr. Santi Kulprathipanja who gave me a valuable opportunity to do this project. They also provided me with invaluable advice, unflinching encouragement, patience, and support in various ways throughout my graduate thesis. Their motivation and help contributed tremendously to the successful completion of the project.

Apart from my advisor and co-advisor, I would like to extend my sincere thanks to the thesis committees: Prof. Apanee Luengnaruemitchai and Dr. Tanate Danuthai for kindly serving on my thesis committee. Their suggestions are certainly important and helpful for completion of this thesis.

I am particularly grateful for the 90th Anniversary of Chulalongkorn University Scholarship (GCUGR1125643050M) for providing financial support throughout this research. Also, thanks to M.S. partial scholarship for tuition support provided by The Petroleum and Petrochemical College.

I'm extremely grateful to the help provided by Dr. Katipot Inkong. This research would not have been possible without his generous support and valuable information. Additionally, thanks should also go to Miss. Viphada Yodpetch, Mr. Siravich Junthong, Mr. Chakorn Viriyakul, and Mr. Kan Jeenmuang, for all their support.

Finally, I most gratefully acknowledge my parents and my friends for their support throughout the period of MS study.

Chuvich Chaovarin

TABLE OF CONTENTS

	Page
ABSTRACT (THAI)	iii
ABSTRACT (ENGLISH).....	iv
ACKNOWLEDGEMENTS	v
TABLE OF CONTENTS	vi
LIST OF TABLES	viii
LIST OF FIGURES	ix
CHAPTER 1 INTRODUCTION	1
CHAPTER 2 THEORETICAL BACKGROUND AND LITERATURE REVIEW	5
2.1 Natural Gas	5
2.2 Natural Gas Storage	6
2.2.1 <u>Compress Natural Gas (CNG)</u>	6
2.2.2 <u>Liquefied Natural Gas (LNG)</u>	6
2.2.3 <u>Adsorbed Natural Gas (ANG)</u>	6
2.3 Gas Hydrates.....	7
2.4 Gas Hydrate Structures	8
2.4.1 <u>Structure I (sI)</u>	9
2.4.2 <u>Structure II (sII)</u>	9
2.4.3 <u>Structure H (sH)</u>	9
2.5 Hydrate Formation.....	10
2.5.1 <u>Hydrate Nucleation</u>	11
2.5.2 <u>Hydrate Growth</u>	11
2.6 Hydrate Dissociation	12
2.6.1 <u>Thermal Stimulation</u>	12
2.6.2 <u>Depressurization</u>	13
2.6.3 <u>Chemical Injection</u>	14

2.7 Enhancing the Rate of Hydrate Formation	14
2.8 Hydrate Promoters	15
2.8.1 <u>Surfactant</u>	15
2.8.2 <u>Amino Acid</u>	17
CHAPTER 3 EXPERIMENTAL.....	23
3.1 Materials and Equipment.....	23
3.1.1 <u>Chemicals</u>	23
3.1.2 <u>Equipment</u>	23
3.2 Experimental Section.....	23
3.2.1 <u>Experimental Apparatus</u>	23
3.2.2 <u>Hydrate Formation Experiment</u>	25
3.2.3 <u>Hydrate Dissociation Experiment</u>	26
CHAPTER 4 RESULT AND DISCUSSION	28
4.1 Effect of L-valine on Methane Hydrate Formation.....	29
4.2 Effect of L-leucine on Methane Hydrate Formation.....	38
4.3 Effect of L-methionine on Methane Hydrate Formation	45
4.4 Comparative Effect of Amino Acids on Methane Hydrate Formation.....	52
4.5 Hydrate Dissociation	54
CHAPTER 5 CONCLUSION AND RECOMMENDATIONS	62
5.1 Conclusion	62
5.2 Recommendations.....	62
APPENDIX.....	63
Appendix A Graphical Abstract	63
REFERENCES	64
VITA.....	74

LIST OF TABLES

Table 2.1 Typical composition of natural gas	5
Table 2.2 Lists the properties of the three common unit crystals	9
Table 2.3 Hydropathy index of amino acids	18
Table 4.1 Experimental results for methane hydrate formation using different L-valine concentrations at 8 MPa and 277.2 K	30
Table 4.2 Experimental results for methane hydrate formation using different L-leucine concentrations at 8 MPa and 277.2 K	39
Table 4.3 Experimental results for methane hydrate formation using different L-leucine concentrations at 8 MPa and 277.2 K	46
Table 4.4 Experimental results for methane hydrate formation using fresh and reused solutions 8 MPa and 277.2 K	60

LIST OF FIGURES

Figure 2.1 Burning of methane hydrate sample.....	7
Figure 2.2 Common clathrate hydrate structures	8
Figure 2.3 Overview of hydrate formation	10
Figure 2.4 Hydrate formation schematic.....	11
Figure 2.5 Schematic diagram of methane hydrate phase equilibrium.....	12
Figure 2.6 Schematic diagram of hydrate dissociation process under thermal stimulation.....	13
Figure 2.7 Schematic diagram of the hydrate dissociation process under depressurization	13
Figure 2.8 Detailed diagram of a hybrid combinatorial approach for hydrate formation.....	15
Figure 2.9 Cumulative methane uptake as a function of time in the presence of (a) SDS, (b) DTAC, (c) DAH, and (d) DN2Cl.....	16
Figure 2.10 Foam formation during the hydrate dissociation using SDS as a kinetic promoter.....	17
Figure 2.11 Methane uptake kinetics for bulk water and L-leucine aqueous solutions at 9.5 MPa and 273 K	19
Figure 2.12 Morphology of methane hydrate formation using 0.3 wt% L-leucine with observed methane bubble.....	20
Figure 2.13 Comparison of hydrate growth profiles for 0.3 wt% of different amino acids at 275.2 K and starting pressure of 10 MPa.....	20
Figure 2.14 Comparison of surfactant and amino acids as effective kinetic hydrate promoters (a) general surfactant structure, (b) general hydrophobic amino acid structure, (c) foam formation on the hydrates dissociation in 0.3 wt% SDS solution (d) absence of any foam formation on the hydrate dissociation in 0.3 wt% leucine solution.....	21
Figure 2.15 Normalized gas uptake calculation for amino acids at 7 and 10 MPa and 1°C at 3000 ppm concentration	22
Figure 2.16 Induction time t_0 of amino acid at the initial operating pressure of 7 and 10 MPa, and isothermal temperature scheme (1°C)	22

Figure 3.1 Schematic of (a) experimental apparatus and (b) cross-section of window crystallizer.....	24
Figure 4.1 Structure of nonpolar amino acids (a) L-valine, (b) L-leucine, and (c) L-methionine.....	28
Figure 4.2 Effects of L-valine concentrations on (a) induction time and NR_{30} and (b) methane uptake and water to hydrate conversion on methane hydrate formation at 8 MPa and 277.2 K.	31
Figure 4.3 Average methane uptake profiles during methane hydrate formation using different concentrations of L-valine at 8 MPa and 277.2 K.	32
Figure 4.4 Morphology observation during methane hydrate formation using different L-valine concentrations at 8 MPa and 277.2 K.	36
Figure 4.5 Zoomed morphology of methane hydrate formation in the presence of L-valine.	37
Figure 4.6 Effects of L-leucine concentrations on (a) induction time and NR_{30} and (b) methane uptake and water to hydrate conversion on methane hydrate formation at 8 MPa and 277.2 K.	40
Figure 4.7 Average methane uptake profiles during methane hydrate formation using different L-leucine concentration at 8 MPa and 277.2 K.	41
Figure 4.8 Morphology observation during methane hydrate formation using different L-leucine concentrations at 8 MPa and 277.2 K.	43
Figure 4.9 Zoomed morphology of methane hydrate formation in the presence of L-leucine.	44
Figure 4.10 Effects of L-methionine concentrations on (a) induction time and NR_{30} and (b) methane uptake and water to hydrate conversion on methane hydrate formation at 8 MPa and 277.2 K.	47
Figure 4.11 Average methane uptake profiles during methane hydrate formation using different L-methionine concentration at 8 MPa and 277.2 K.	48
Figure 4.12 Morphology observation during methane hydrate formation using different L-methionine concentrations at 8 MPa and 277.2 K.	50
Figure 4.13 Zoomed morphology of methane hydrate formation in the presence of L-methionine.....	51
Figure 4.14 Average methane uptake profiles during methane hydrate formation using (a) 0.25 wt%, (b) 0.50 wt%, and (c) 1.00 wt% of different amino acids at 8 MPa and 277.2 K.	52

Figure 4.15 Average normalized methane recovery profiles during methane hydrate dissociation in the presence of (a) different amino acid concentration and (b) different amino acids.55

Figure 4.16 Morphology observations during methane hydrate dissociation using different amino acids with different concentrations at 8 MPa and 277.2 K.58

Figure 4.17 Final methane uptakes achieved from the fresh and reused solutions of 1.00 wt% L-valine, L-leucine, and L-methionine at 8 Mpa and 277.2 K.59



CHAPTER 1

INTRODUCTION

Natural gas, the cleanest-burning fossil fuel, is one of the most important sources of energy. Natural gas demand is expected to increase continuously from 2019 to 2025. The forecast expects an average annual growth rate of 1.5% during this period, reported by EIA (2020). From the widely used natural gas, storage and transportation are the issues that need to be considered. Compressed natural gas (CNG) is one of approaches to store natural gas in a smaller volume. But under the high-pressure condition, safety must be considered as it is flammable. Another approach is liquefied natural gas (LNG). It has a high volumetric storage capacity with the ease in transportation. But it requires a huge amount of energy to maintain at low temperature (111 K). To escape these drawbacks, there is an interest in storing natural gas in a solid form, as solidified natural gas (SNG) via clathrate hydrates (Thomas and Dawe, 2003; Veluswamy *et al.*, 2018).

Gas hydrates, also known as clathrate hydrates, are solid crystalline inclusion compounds containing water and gas molecules such as methane, ethane, or propane (Carroll, 2020; Sloan Jr and Koh, 2007). They form a solid network of hydrogen-bond water molecules at high pressure and low temperature. Guest gases are stored in cavities between their molecules (Costandy *et al.*, 2015). There are three main structures of gas hydrates; cubic structure I (sI), cubic structure II (sII), and the hexagonal structure (sH) (Sloan Jr and Koh, 2007; Strobel *et al.*, 2009). After Makogon's discovery of natural gas hydrates as an energy resource in 1965, there has been intense research into the gas hydrate formation, which has become an interesting approach to natural gas storage (Makogon, 1981; Veluswamy *et al.*, 2018). Furthermore, there are other applications of gas hydrates such as carbon dioxide capture, separation processes, and water desalination (Babu *et al.*, 2018; Eslamimanesh *et al.*, 2012; Sun and Kang, 2016).

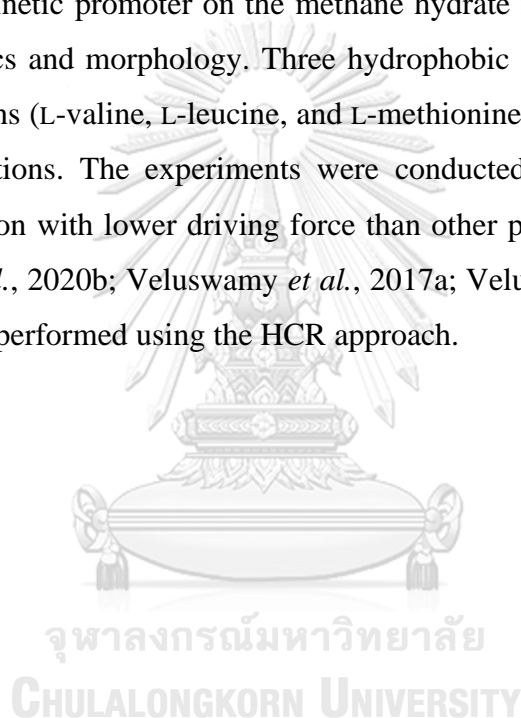
Clathrate hydrates for storing natural gas as SNG are very safe and environmentally benign. In addition, as compared to other approaches, the storage conditions require less energy (Veluswamy *et al.*, 2018). However, clathrate hydrates

are limited by their slow rate of hydrate formation. Therefore, there are challenges to overcome in order to propel the clathrate hydrate technology for gas storage (Veluswamy *et al.*, 2016b). Increasing mass transfer by changing reactor design is one method to improve the hydrate formation rate. Stirred tank reactors are known to provide high initial hydrate formation rates but low conversion of water to hydrates due to unintentional hydrate formation, preventing the efficient mass transfer of the gas through the gas-liquid interface. On the other hand, an unstirred tank reactor results in higher final gas uptake and higher water to hydrate conversions for methane hydrate formation with kinetic promoters (Linga *et al.*, 2012; Zhong *et al.*, 2015). Veluswamy *et al.* (2017a) found that the hybrid combinatorial reactor (HCR) approach, a simple combination of stirred and unstirred reactor configurations, effectively improved the kinetics of methane hydrate formation in the presence of 0.3 wt% L-leucine. The HCR involves stirring the reactor contents until hydrate nucleation occurs. The hydrate growth then continues in an unstirred state. Using kinetic hydrate promoters is yet another possible method to improve the hydrate formation rate. Surfactants have been widely reported in the literature as kinetic promoters for hydrate formation (Kalogerakis *et al.*, 1993; Kumar *et al.*, 2015; Veluswamy *et al.*, 2015). Ganji *et al.* (2007) studied the effect of different surfactants on the methane hydrate formation. They found that all surfactant promoters efficiently increased the methane hydrate formation rate and also increased the storage capacity of methane hydrate compared to pure water systems. In particular, sodium dodecyl sulfate (SDS), an anionic surfactant, significantly reduces the induction time. SDS has been reported to be one of the best kinetic promoters because it enhances the mass transfer of gas molecules to the liquid solution by reducing the tension at the gas-liquid interface (Du *et al.*, 2014; Wang *et al.*, 2015; Yoslim *et al.*, 2010). However, the main disadvantage of using SDS as a kinetic promoter is foam formation during the dissociation process. This foam deters the hydrate dissociation, reducing the gas release rate, which is undesirable on a large scale (Veluswamy *et al.*, 2016a). In addition, they are not environmentally friendly. Therefore, some studies have attempted to reduce the foam generation in the SDS solutions (Pandey *et al.*, 2018; Viriyakul *et al.*, 2021) or find other compounds with similar properties.

Amino acids are promising alternatives as they are biomolecules and have a similar chemical structure to surfactants. Amino acids consist of amine ($-NH_2$) and carboxylic ($-COOH$) functional groups along with a characteristic side chain. The various side chains make amino acids with different properties, which can be classified into polar (hydrophilic) and nonpolar (hydrophobic) (Bavoh *et al.*, 2019; Bhattacharjee and Linga, 2021). In the field of gas storage, amino acids are used as a kinetic promoter to improve the rate of hydrate formation. Liu *et al.* (2015) studied the promotion effect of natural amino acids on the kinetics of methane hydrate formation. 0.5 wt% L-leucine can promote methane hydrate formation at a high rate and capacity of 143 mg/g at 9.5 MPa and 273 K. Veluswamy *et al.* (2016a) studied the morphology of methane hydrate formation and dissociation in the presence of amino acid. During the methane hydrate formation using L-leucine, an interesting characteristic called “methane bubble” in the bulk solution with a “breathing effect” was observed. These phenomena were attributed to the enhanced methane hydrate formation kinetics. During the methane hydrate dissociation, no foam formation in the L-leucine solution was detected, unlike in the SDS solution. Furthermore, Veluswamy *et al.* (2017b) studied the effect of three different amino acids (tryptophan (nonpolar), histidine (polar), and arginine (polar)) on the kinetics of methane hydrate formation. The induction time was low for all amino acids. But at the same concentration, the nonpolar hydrophobic amino acids (L-tryptophan and L-leucine) significantly enhanced the methane hydrate formation with similar performance in both stirred and unstirred reactor configurations. Pandey *et al.* (2020b) observed that hydrophobic amino acids (L-methionine and L-valine) showed higher methane uptake and lower induction time than hydrophilic amino acids (L-histidine and L-arginine) at the same concentration. In addition, they investigated methane hydrate formation in unconsolidated sediments (silica sand) using biofriendly amino acids. Similar to their previous studies, hydrophobic amino acids (L-valine and L-methionine) served as an effective kinetic promoter for methane hydrate formation, exhibiting comparable kinetic promotion performance to the surfactant SDS (Pandey *et al.*, 2020a).

However, the effect of amino acids on the methane gas hydrates has not yet been fully understood as each amino acid has different properties such as polarity, hydrophobicity index, and side chain characteristics (Bavoh *et al.*, 2019; Bhattacharjee

and Linga, 2021; Veluswamy *et al.*, 2017b). According to our group's previous study (Inkong *et al.*, 2022b; Jeenuang *et al.*, 2021) using amino acids (L-valine, L-leucine, and L-methionine) as a co-promoter on the mixed methane-THF hydrate formation, the amino acids significantly increased the hydrate formation rate. It would be interesting to study in detail the macroscopic kinetics of pure methane hydrate formation in the presence of amino acids, including the morphology during the process, combined with the HCR approach for hydrate formation, has not been studied in depth. Therefore, the objective of this research was to investigate the role of amino acid as a kinetic promoter on the methane hydrate formation and dissociation in terms of kinetics and morphology. Three hydrophobic amino acids with different aliphatic side chains (L-valine, L-leucine, and L-methionine) were used in this study at various concentrations. The experiments were conducted at 8 MPa and 277.2 K, which is a condition with lower driving force than other previous studies (Liu *et al.*, 2015; Pandey *et al.*, 2020b; Veluswamy *et al.*, 2017a; Veluswamy *et al.*, 2017b). The experiments were performed using the HCR approach.



CHAPTER 2

THEORETICAL BACKGROUND AND LITERATURE REVIEW

2.1 Natural Gas

Natural gas, a type of fossil fuel, has been formed by the decomposition of organic matter accumulated over the past millions of years and is stored under pressure in rock reservoirs in the Earth's crust. The principal component of natural gas is methane. Other components are paraffinic hydrocarbons such as ethane, propane, and butanes, as shown in Table 2.1.

Table 2.1 Typical composition of natural gas (Mokhatab and Poe, 2012)

Name	Formula	Volume (%)
Methane	CH ₄	> 85
Ethane	C ₂ H ₆	3 - 8
Propane	C ₃ H ₈	1 - 2
Butane	C ₄ H ₁₀	< 1
Pentane	C ₅ H ₁₂	< 1
Carbon dioxide	CO ₂	1 - 2
Hydrogen sulfide	H ₂ S	< 1
Nitrogen	N ₂	1 - 5
Helium	He	< 0.5

In the past, natural gas was often an unwelcome by-product, as it interfered with the drilling of crude oil. But after a shortage of crude oil in the 70s, natural gas has become the world's major energy source. It is used primarily as fuel and as a raw material in manufacturing. Natural gas is considered a clean fuel that is environmentally friendly when compared to other fossil fuels. The environmental qualities over coal or crude oil, meaning its sulfur dioxide emissions are negligible, or the levels of nitrous oxide and carbon dioxide emissions are lower. So, it can reduce problem of acid rain, ozone layer, or greenhouse gases (e.g., SO₂, CO, CO₂) (Mokhatab and Poe, 2012). According to international energy agency (IEA) data,

global natural gas consumption is still increasing. Although it dropped around 2% in 2019-2021 due to the COVID-19 pandemic (EIA, 2021).

2.2 Natural Gas Storage

In the past several years, natural gas has been popular and attractive as a green alternative energy source. The rate of natural gas consumption will continuously grow until 2040. Natural gas is used in daily life for cooking, vehicles, and industrial processes. Therefore, natural gas storage technologies are continually evolving to be consistent with global energy demand (Veluswamy *et al.*, 2018).

2.2.1 Compress Natural Gas (CNG)

CNG is a simple method to store natural gas by compressing it under 20-25 MPa and 293.2 K. CNG can be used readily without any additional preparation steps. However, the major disadvantage is safety concern, as natural gas can be flammable and explosive. The storage tanks must be thick enough to withstand high pressure conditions and have safety valve systems installed, which are high cost. In addition, CNG has a relatively low volumetric storage capacity in comparison to other technologies.

2.2.2 Liquefied Natural Gas (LNG)

LNG is produced by cooling natural gas until it is converted to a liquid form. Due to its high volumetric storage capacity, LNG is suitable for use in large-scale and long-distance transportation. However, it requires a lot of energy to maintain at a low temperature (113.2 K) to store in liquid form via a cooling system, as well as a high cost of storage equipment.

2.2.3 Adsorbed Natural Gas (ANG)

ANG is a possible method of storage and transportation by adsorbing natural gas on high porous materials such as activated carbon, graphene, metal organic frameworks (MOFs), etc. It requires low pressure storage (6.5 MPa, lower than in CNG). However, it cannot be used commercially because the price of the

adsorbent is expensive and adsorbent contamination is observed when using many cycles.

To overcome these drawbacks, such as low volumetric storage capacity, high equipment cost, and flammability concerns, there is an interest in storing natural gas in the solid form as solidified natural gas (SNG) via clathrate hydrates (Thomas and Dawe, 2003; Veluswamy *et al.*, 2018).

2.3 Gas Hydrates

Gas hydrates or clathrate hydrates are crystalline inclusion compounds of water (host) and gas molecules (guest) such as methane, ethane, or propane. They form spontaneously by a solid network of hydrogen-bonded water molecules at high pressure and low temperature. Guest gases are stored in cavities between their molecules (Costandy *et al.*, 2015). In the past, the presence of water in natural gas was a serious industrial problem due to the formation of gas hydrates by water. These solids interfere with the piping system (Hammerschmidt, 1934). Since the discovery of methane hydrates in the deep sea, gas hydrates have been gaining attention as a gas storage technology. Gas hydrates will be an energy source with enormous potential and will be used in many applications such as natural gas storage and transportation, carbon dioxide capture, and desalination processes (Eslamimanesh *et al.*, 2012; Sharma *et al.*, 2019; Sun and Kang, 2016).



Figure 2.1 Burning of methane hydrate sample (Siažik *et al.*, 2017).

2.4 Gas Hydrate Structures

Gas hydrates are not chemical compounds. They form spontaneously at high pressure and low temperature. Guest gases stay inside hydrogen-bonded water cages and interact with them by Van der Waals forces, which is physical bonding (Veluswamy *et al.*, 2018). The structure is three-dimensional. Guest gases (e.g., hydrogen, methane, carbon dioxide) have different molecule sizes, resulting in structural differences. There are three main structures of gas hydrates: cubic structure I (sI), cubic structure II (sII), and the hexagonal structure (sH) (Sloan Jr and Koh, 2007; Strobel *et al.*, 2009).

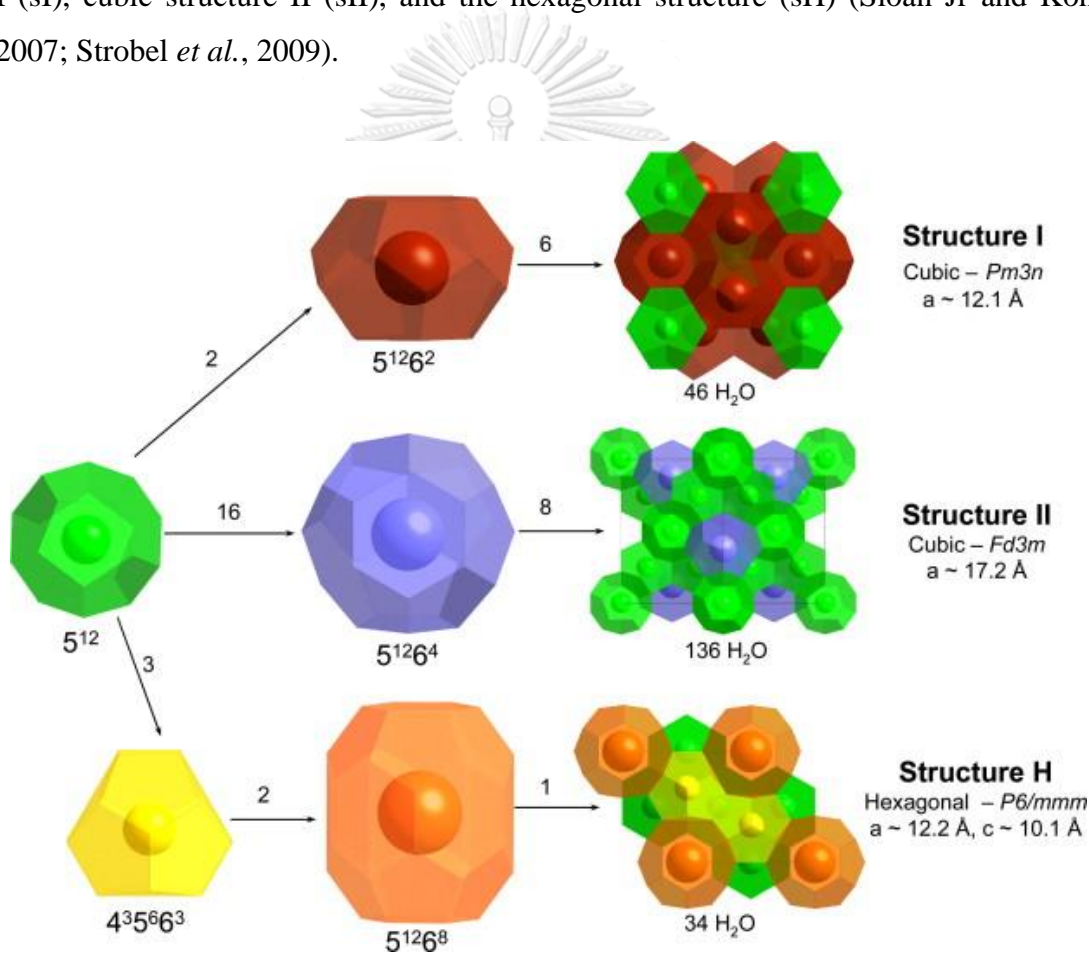


Figure 2.2 Common clathrate hydrate structures (Strobel *et al.*, 2009).

Table 2.2 Lists the properties of the three common unit crystals (Sloan, 2003)

Hydrate crystal structure	sI		sII		sH		
	Small	Large	Small	Large	Small	Medium	Large
Description	5^{12}	$5^{12}6^2$	5^{12}	$5^{12}6^4$	5^{12}	$4^35^66^3$	$5^{12}6^8$
Number of cavities per unit cell	2	6	16	8	3	2	1
Average cavity radius (Å)	3.95	4.33	3.91	4.73	3.91	4.06	5.71
Coordination number	20	24	20	28	20	20	36
Number of water per unit cell	46		136		34		

2.4.1 Structure I (sI)

In sI, it is a cubic unit cell. There are 2 small pentagonal dodecahedron (5^{12}) combined with 6 large tetrakaidecahedrons ($5^{12}6^2$) cages. The sI hydrates can contain 8 guest gas molecules, which are usually small molecules such as methane, ethane, and carbon dioxide (Sloan, 2003).

2.4.2 Structure II (sII)

In the sII, it is a face-centered cubic unit cell. 136 water molecules form frameworks around 16 small pentagonal dodecahedron (5^{12}) and 8 large hexakaidodecahedron ($5^{12}6^4$) cages (Mao *et al.*, 2002). 24 guest gas molecules such as propane and i-butane can be accommodated in these cages.

2.4.3 Structure H (sH)

In sH, it is formed by using 34 water molecules. There are 3 types of cages: 3 small pentagonal dodecahedron (5^{12}), 2 medium dodecahedrons ($4^35^66^3$), and 1 large icosahedron ($5^{12}6^8$) cages (Lederhos *et al.*, 1992). These cages make sH hydrates store larger amounts of guest gas molecules than sI and sII hydrates. The gas

storage capacity of sH hydrates is approximately 25% greater than sII hydrates (Shin *et al.*, 2011). The large guest gas molecule (e.g., cycloheptane) can be encapsulated in 1 large cage (Sloan, 2003).

Each sI and sII have two cavity sizes (small and large). Although sI hydrates can contain more guest gas, for natural gas storage (or methane storage), sI is preferred due to more stability (Buffett, 2000).

2.5 Hydrate Formation

Hydrate formation occurs at high pressure and low temperature. It is usually observed at 6-10 MPa and 273.5 K (Ohmura *et al.*, 2005). While the formation of hydrate occurs, a decrease in pressure and an increase in temperature are observed as it is an exothermic process (Zhang *et al.*, 2017). The process of hydrate formation can be divided into two steps: a nucleation phase and a growth phase, which is the same as the crystallization process. The hydrate formation process starts when the gas uptake increases, then it grows until the hydrate structure stabilizes (Khurana *et al.*, 2017).

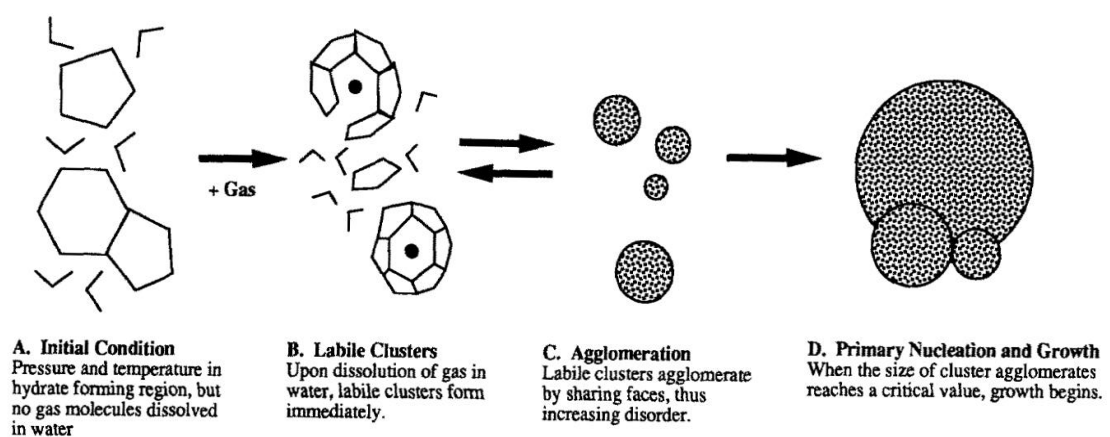


Figure 2.3 Overview of hydrate formation (Christuansen and Sloan, 1994).

2.5.1 Hydrate Nucleation

Hydrate nucleation is a microscopic process. The hydrate formation starts at the gas-liquid interface to form small hydrate crystals, then reaches the growth phase (You *et al.*, 2019). In the beginning, the growth of hydrates is relatively low due to meta-stability, or natural inhibition, which prevents the hydrate formation (Lederhos *et al.*, 1996). Figure 2.4 shows the schematic of hydrate formation. The first step in nucleation, gas uptake increases without gas dissolved into water, call dissolution phase. After that, a supersaturated phase occurs when the pressure and temperature are in suitable conditions. And end with the critical nucleus phase. The time between super saturation and the critical nucleus phase is called the induction time (Khurana *et al.*, 2017).

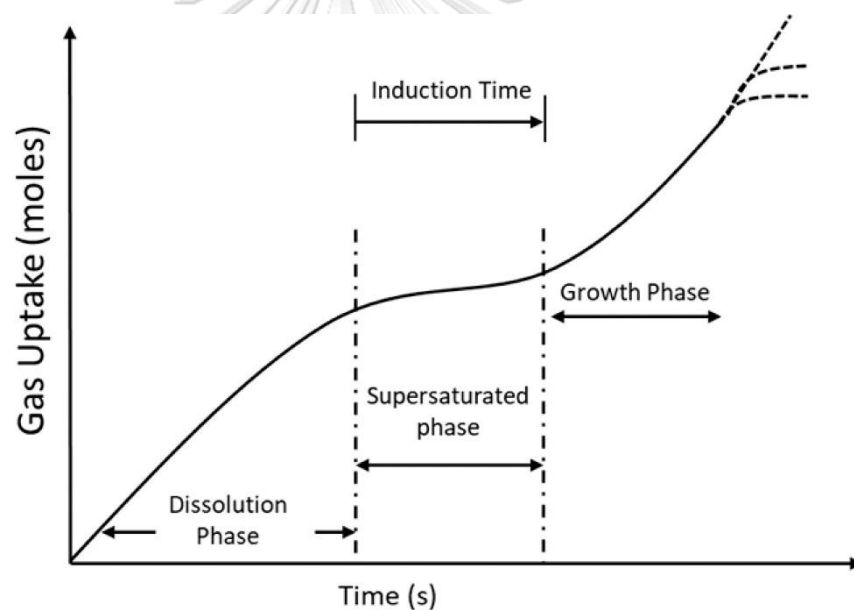


Figure 2.4 Hydrate formation schematic (Khurana *et al.*, 2017).

2.5.2 Hydrate Growth

After the hydrate nucleation step, the process of crystal growth occurs to form gas hydrates. Morlat *et al.* (1976) studied the kinetics of ethylene hydrate formation and proposed that there are two steps in hydrate growth. First, the larger hydrate cavities are formed, followed by smaller cavities. The guest gas is transported to the liquid phase and temporarily occupies the cavities. After that, the guest gas is filled permanently. Then, hydrate structures become stable.

2.6 Hydrate Dissociation

Hydrate dissociation is an endothermic process. Hydrates are stable when the pressure-temperature conditions are above the hydrate equilibrium curve. The conditions below the equilibrium curve cause hydrate dissociation. The guest gases in the hydrate structures are dispersed into gas and water phases (Yang *et al.*, 2019). There are three independent approaches commonly used to dissociate gas hydrates: thermal stimulation, depressurization, and inhibitor injection (Kondori *et al.*, 2017), as shown in Figure 2.5.

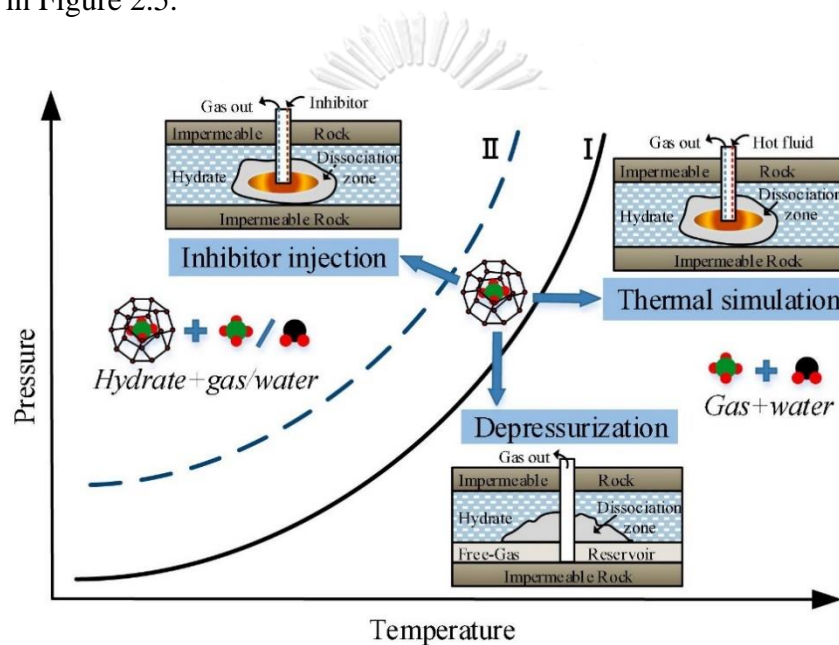


Figure 2.5 Schematic diagram of methane hydrate phase equilibrium (Yang *et al.*, 2019).

2.6.1 Thermal Stimulation

The thermal stimulation method can dissociate hydrates by heating. In general, there are three steps in this method, as shown in Figure 2.6. This method is limited by heat transfer because the dissociated water forms a thin liquid film on the surface of the remaining hydrates, which blocks heat transfer.

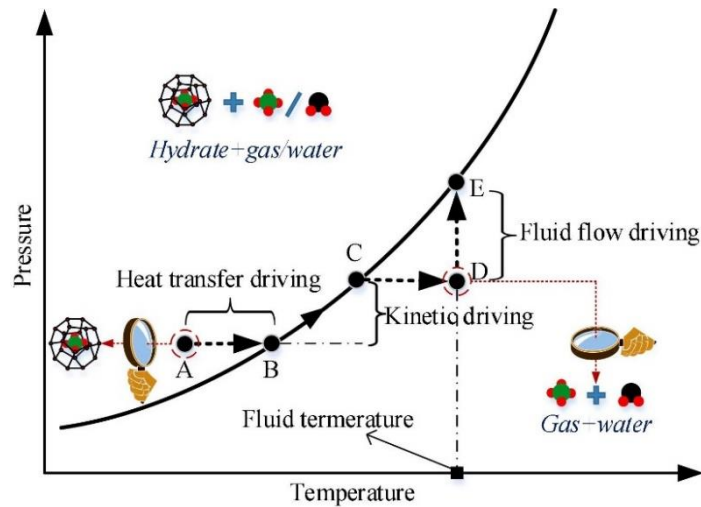


Figure 2.6 Schematic diagram of hydrate dissociation process under thermal stimulation (Yang *et al.*, 2019).

2.6.2 Depressurization

The pressure reduction method dissociates hydrates by reducing the pressure in the system. There are three steps in this method, shown in Figure 2.7. After reducing pressure, the temperature drops due to endothermic processes. Therefore, heat transfer and kinetic forces are the main factors in the dissociation hydrates in this method.

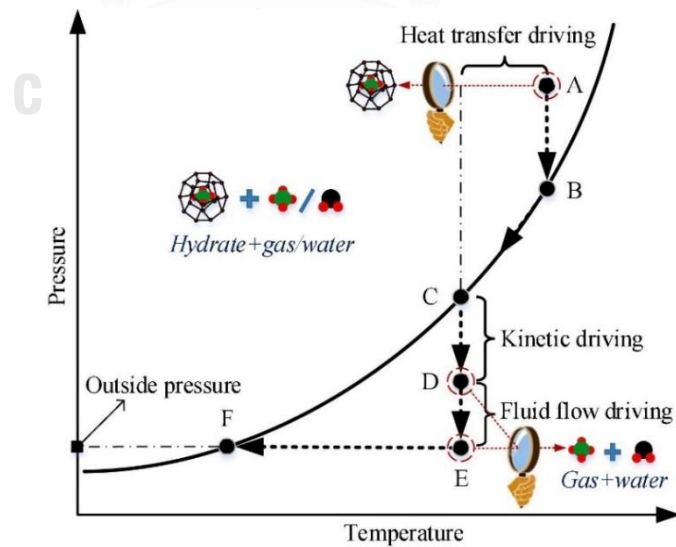


Figure 2.7 Schematic diagram of the hydrate dissociation process under depressurization (Yang *et al.*, 2019).

2.6.3 Chemical Injection

Chemical injection dissociates hydrates by injecting the thermodynamic inhibitors with strong hydrogen bonding (e.g., ethylene glycol and methanol). They can interrupt the hydrate equilibrium (Kondori *et al.*, 2017).

2.7 **Enhancing the Rate of Hydrate Formation**

Although clathrate hydrates as a natural gas storage technology have many advantages, they have some limitations, especially the low rate of hydrate formation. Therefore, there are challenges to overcome in order to propel the commercialization of clathrate hydrate technology for natural gas storage (Veluswamy *et al.*, 2016b). Increasing mass transfer by changing reactor design is one method to improve the hydrate formation rate. Stirred tank reactors are known to provide high initial hydrate formation rates but low conversion of water to hydrates due to unintentional hydrate formation. This prevents the efficient mass transfer of the gas through the gas-water interface. On the other hand, the final gas uptake and final conversion were found to be significantly higher in the unstirred reactor (Linga *et al.*, 2012; Zhong *et al.*, 2015). Veluswamy *et al.* (2017a) found that the hybrid method, a simple combination of stirred and unstirred reactor configurations, effectively improved the kinetics of methane hydrate formation. It combines the advantages of both reactor configurations, as shown in Figure 2.8. The hybrid method involves stirring the reactor contents until hydrate nucleation occurs, then continuing the hydrate growth in an unstirred.

Novel combinatorial hybrid approach to reduce nucleation stochasticity during methane hydrate formation

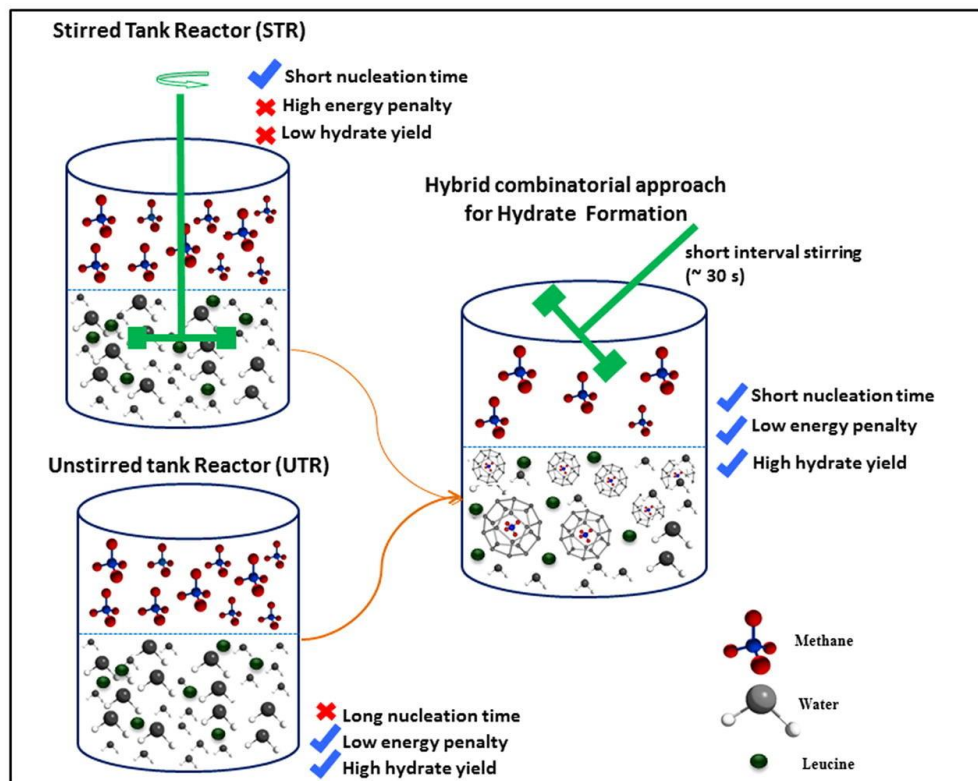


Figure 2.8 Detailed diagram of a hybrid combinatorial approach for hydrate formation (Veluswamy *et al.*, 2017a).

2.8 Hydrate Promoters

Hydrate promoters are additives that are used to enhance the rate of hydrate formation without influencing the thermodynamics. They can improve the dispersion of gas into liquid solutions by reducing the tension at the interface. Examples of kinetic promoters are surfactants, amino acids, polymers, and starches.

2.8.1 Surfactant

Kalogerakis *et al.* (1993) studied the effect of surfactants on hydrate formation kinetics by using anionic and nonionic surfactants. Surfactants, with concentrations near CMC levels, can increase the rate of hydrate formation with no effect on the thermodynamics. In addition, the rate of hydrate formation in anionic

surfactants is higher than in nonionic surfactants. Sodium dodecyl sulfate (SDS), which is an anionic surfactant, is recognized as the best surfactant kinetic promoter.

Zhang *et al.* (2007) studied the kinetics of methane hydrate formation from SDS solution. SDS dramatically reduced the induction time for methane hydrates. In addition, the rate of methane hydrate formation was analyzed. SDS solution transport to the porous hydrate layer on the reactor wall during the hydrate growth period caused the gas-liquid interfacial area to increase. Therefore, the rate of methane hydrate formation increased.

Du *et al.* (2014) studied the effects of ionic surfactants such as sodium dodecyl sulfate (SDS), dodecylamine hydrochloride (DAH), dodecyltrimethylammonium chloride (DTAC) and N-dodecylpropane-1,3-diamine hydrochloride (DN₂Cl) on methane hydrate formation kinetics in a static system. As shown in Figure 2.9, SDS gave higher hydrate growth rates than others and the final methane uptake increased with increasing SDS concentration.

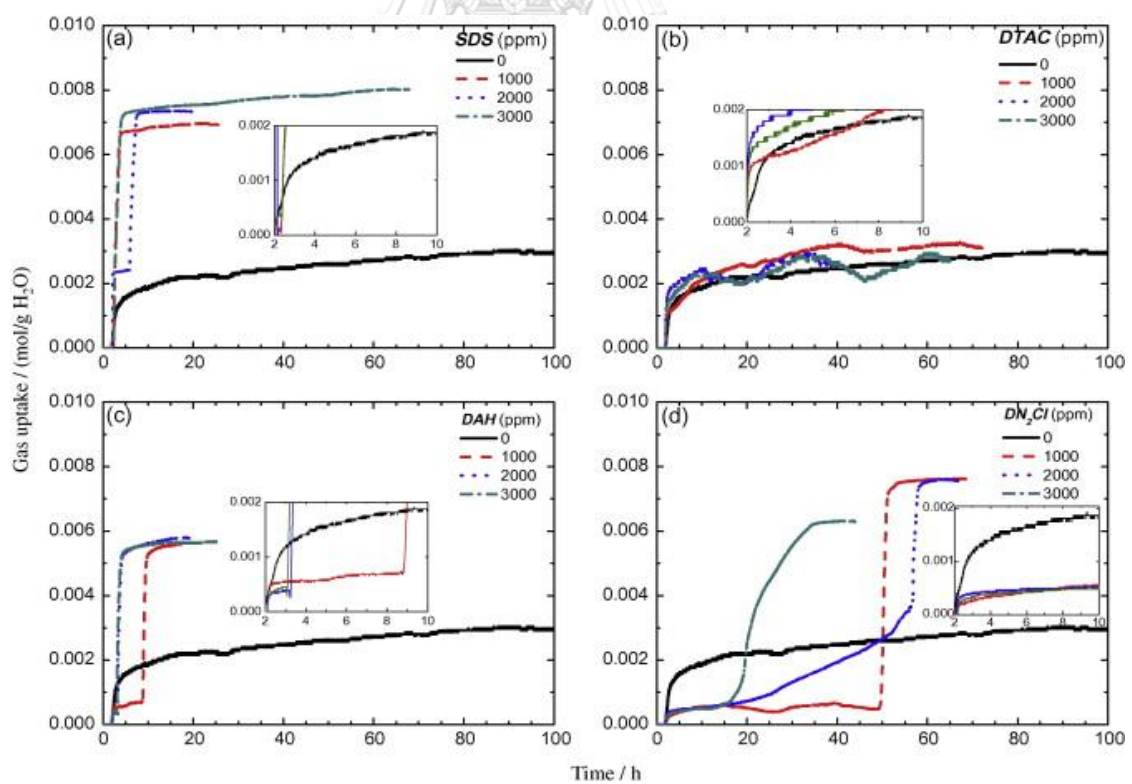


Figure 2.9 Cumulative methane uptake as a function of time in the presence of (a) SDS, (b) DTAC, (c) DAH, and (d) DN₂Cl (Du *et al.*, 2014).

In addition, Wang *et al.* (2015) studied the effects of different anionic surfactants on methane hydrate formation. Due to the lower surface tension and narrow contact angle, SDS had high performance to enhance hydration formation.

However, the main drawback of SDS is the foam formation during the hydrate dissociation, which is undesirable to occur in the process (Veluswamy *et al.*, 2016a), shown in Figure 2.10. And surfactants are also toxic to the environment. Therefore, many researchers are interested in finding a way to reduce foam formation or use other substances instead.

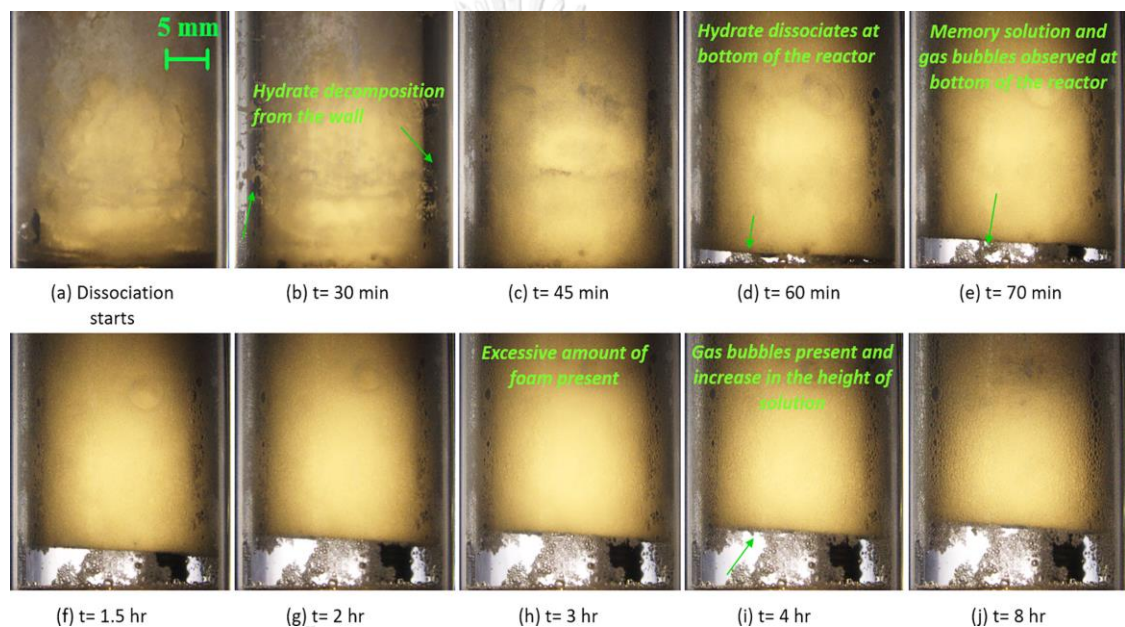


Figure 2.10 Foam formation during the hydrate dissociation using SDS as a kinetic promoter (Pandey *et al.*, 2018).

2.8.2 Amino Acid

Amino acids are organic compounds that consist of an amine ($-\text{NH}_2$) and a carboxylic ($-\text{COOH}$) functional group along with a characteristic side chain. These various side chains give different properties of amino acids, which can be classified into polar (hydrophilic) and nonpolar (hydrophobic). The hydrophobic or hydrophilic properties of an amino acid side chain are ranked using a number called the hydropathy index. The high hydropathy index of amino acids represents more hydrophobicity (Bhattacharjee and Linga, 2021). In the past, amino acids were used

as hydrate inhibitors. The lower hydrophobicity amino acids give better inhibition performance. Although, they are not the best chemical inhibitors, they are environmentally friendly and biodegradable (Naeiji *et al.*, 2014).

Table 2.3 Hydropathy index of amino acids (Mitaku *et al.*, 2002)

Side chain	Hydropathy index
Isoleucine	4.5
Valine	4.2
Leucine	3.8
Phenylalanine	2.8
Cysteine/cystine	2.5
Methionine	1.9
Alanine	1.8
Glycine	-0.4
Threonine	-0.7
Tryptophan	-0.9
Serine	-0.8
Tyrosine	-1.3
Proline	-1.6
Histidine	-3.2
Glutamic acid	-3.5
Glutamine	-3.5
Aspartic acid	-3.5
Asparagine	-3.5
Lysine	-3.9
Arginine	-4.5

In the field of gas storage, amino acids are used as kinetic promoters to improve the rate of hydrate formation. Liu *et al.* (2015) studied the promotion effect of natural amino acids on the kinetics of methane hydrate formation. Figure 2.11 shows different concentrations of L-leucine. 0.5 wt% L-leucine can promote methane

hydrate formation at a high rate, with a capacity of 143 mg/g at 9.5 MPa and 273 K. In addition, foam formation was not observed in the methane hydrate dissociation using L-leucine promoter, unlike using SDS surfactants.

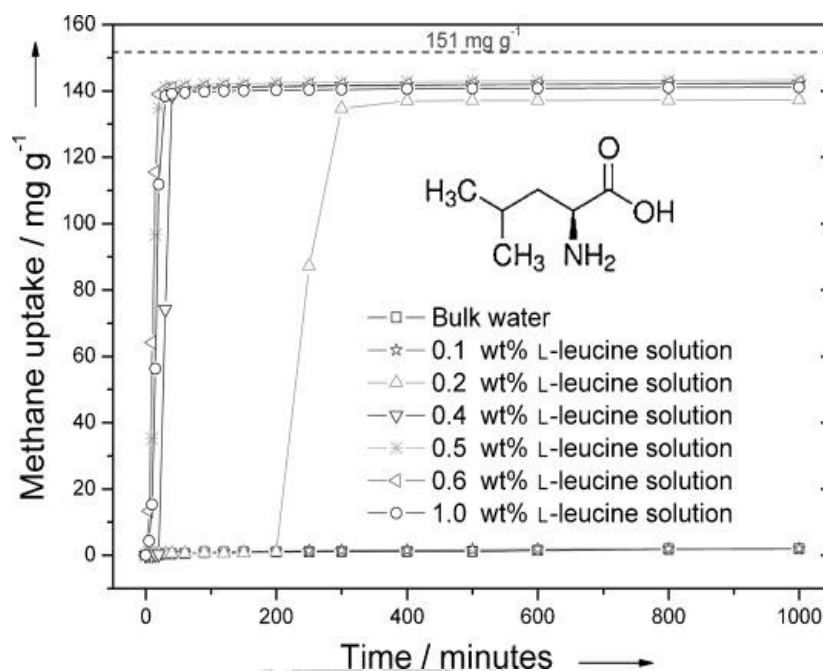


Figure 2.11 Methane uptake kinetics for bulk water and L-leucine aqueous solutions at 9.5 MPa and 273 K (Liu *et al.*, 2015).

Veluswamy *et al.* (2016a) studied the morphology of methane hydrate formation and dissociation in the presence of amino acid. During methane hydrate formation using L-leucine amino acid, they found an interesting characteristic called “methane bubble” in the bulk solution with the assistance of “breathing effect”, as shown in Figure 2.12. These phenomena are attributed to enhance methane hydrate formation kinetics. During methane hydrate dissociation, they observed no foam formation in L-leucine solution but observed it in SDS solution.

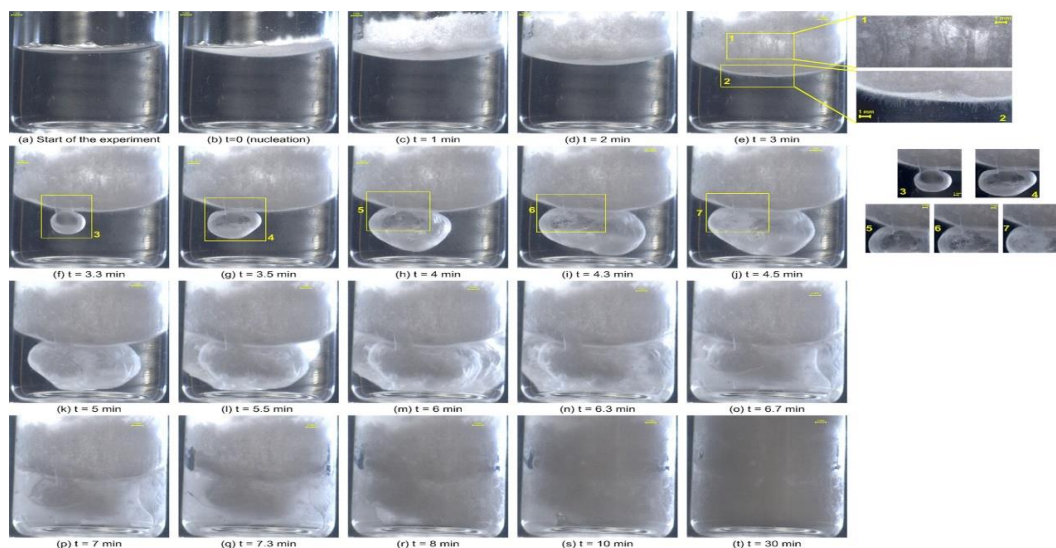


Figure 2.12 Morphology of methane hydrate formation using 0.3 wt% L-leucine with observed methane bubble (Veluswamy *et al.*, 2016a).

Veluswamy *et al.* (2017b) studied the effect of biofriendly amino acids on the kinetics of methane hydrate formation using three different amino acids: tryptophan (nonpolar), histidine (polar), and arginine (polar). The induction time was low for all amino acids. But at the same concentration, nonpolar amino acids (tryptophan, leucine) significantly enhanced methane hydrate formation, as shown in Figure 2.13.

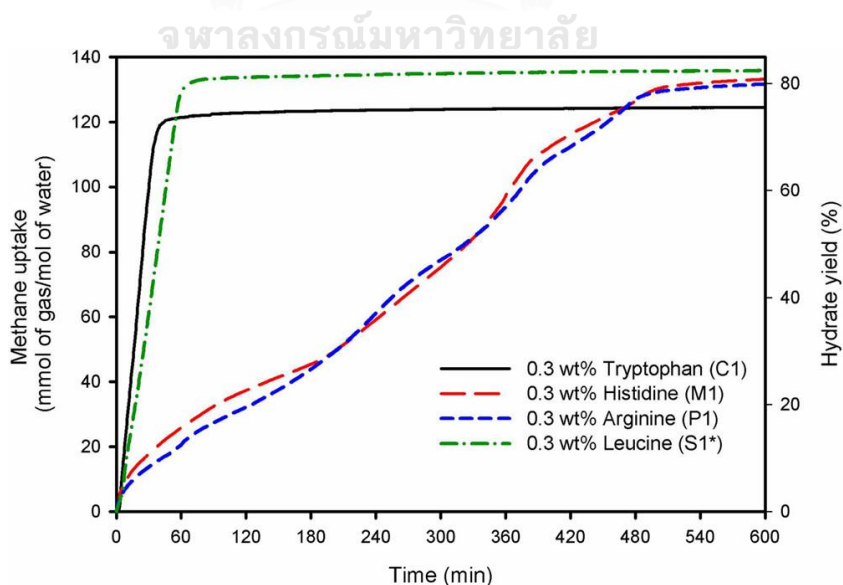


Figure 2.13 Comparison of hydrate growth profiles for 0.3 wt% of different amino acids at 275.2 K and starting pressure of 10 MPa (Veluswamy *et al.*, 2017b).

Figure 2.14 presents the comparison of surfactant and amino acids as effective kinetic hydrate promoters. As mentioned about the foam formation problem, hydrophobic amino acids have similar chemical structure to surfactants, but there is no foam formation in the hydrate dissociation process. Moreover, amino acids are environmentally friendly and inexpensive to synthesize. Therefore, hydrophobic amino acids are the perfect substitute for surfactants as efficient kinetic hydrate promoters (Bhattacharjee and Linga, 2021).

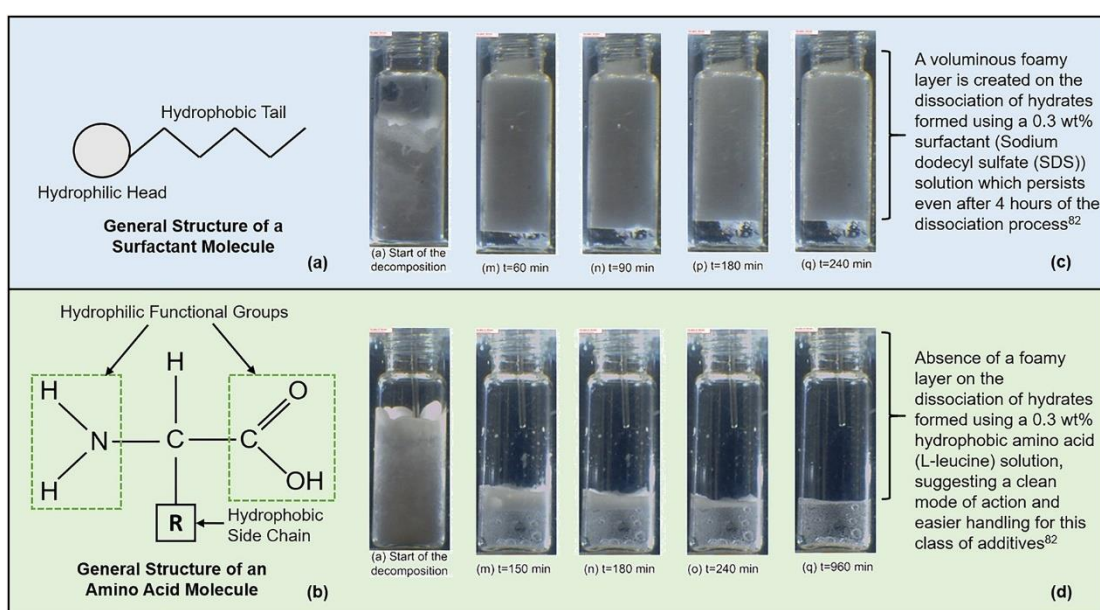


Figure 2.14 Comparison of surfactant and amino acids as effective kinetic hydrate promoters (a) general surfactant structure, (b) general hydrophobic amino acid structure, (c) foam formation on the hydrates dissociation in 0.3 wt% SDS solution (d) absence of any foam formation on the hydrate dissociation in 0.3 wt% leucine solution (Bhattacharjee and Linga, 2021).

For further studies on various amino acids as kinetic promoters for methane hydrate formation, Pandey *et al.* (2020b) observed that hydrophobic amino acids: L-methionine and L-valine used at a concentration of 0.3 wt% showed higher gas uptakes and lower induction times compared to hydrophilic amino acids L-histidine and L-arginine at the same concentration. An increase in the pressure led to a decrease in the induction time due to the increase in the driving force for all amino acids. All results are shown in Figures 2.15 and 2.16. However, the hydrophathy index

of amino acids cannot be used to describe the tendency of the induction time because the induction time does not follow the hydrophobicity ranking. That is L-valine, which has a higher hydropathy index, has a higher induction time than L-methionine. Therefore, it is a matter that must be studied further.

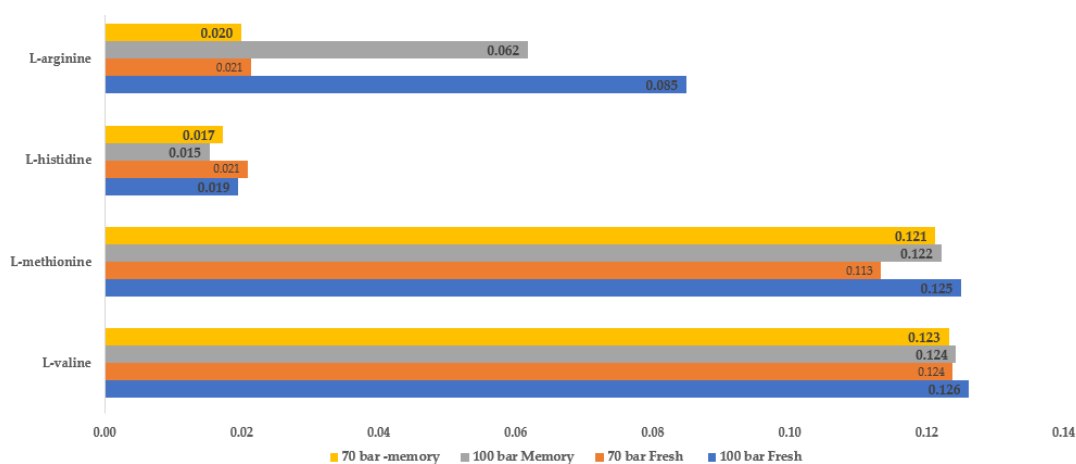


Figure 2.15 Normalized gas uptake calculation for amino acids at 7 and 10 MPa and 1°C at 3000 ppm concentration (Pandey *et al.*, 2020b).

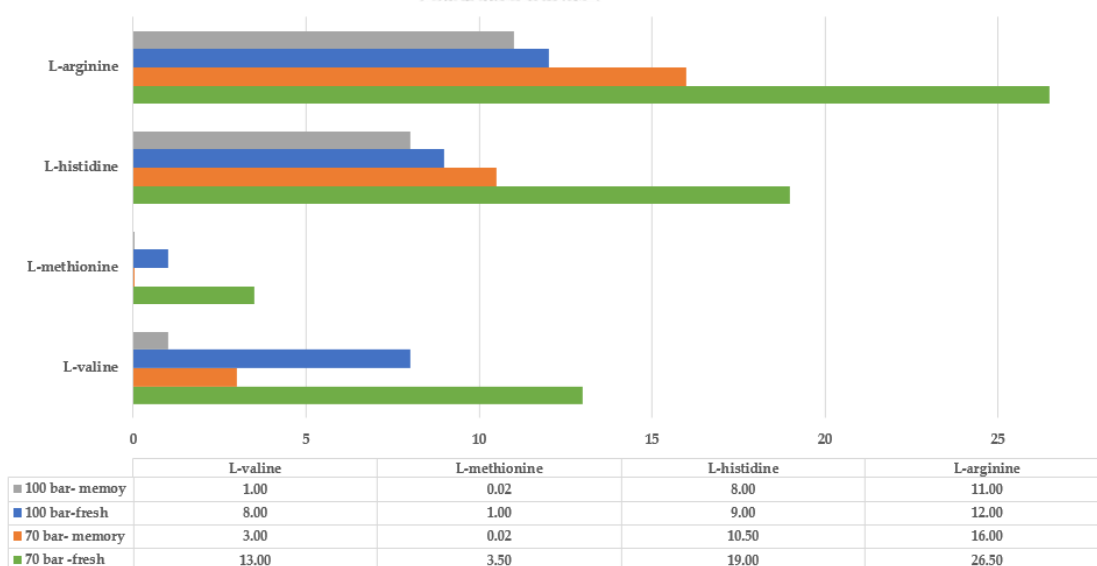


Figure 2.16 Induction time t_0 of amino acid at the initial operating pressure of 7 and 10 MPa, and isothermal temperature scheme (1°C) (Pandey *et al.*, 2020b).

CHAPTER 3

EXPERIMENTAL

3.1 Materials and Equipment

3.1.1 Chemicals

1. Ultra-high purity methane gas (99.99% purity from Linde Public Company, Thailand)
2. Three types of amino acid in the powder form including L-valine, L-leucine, and L-methionine, 99 %, were purchased from Sigma-Aldrich, Singapore.
3. Deionized water

3.1.2 Equipment

1. Crystallizer (CR)
2. Reservoir (R)
3. Personal Computer (PC)
4. Pressure transmitter (PT)
5. External Refrigerator (ER)
6. Thermocouple (TC)
7. Data logger (DL)
8. Video camera (VC)

3.2 Experimental Section

3.2.1 Experimental Apparatus

The schematic of gas hydrate experimental setup is shown in a, which was modified from previous works by our group. All kinetic experiments were carried out in a batch crystallizer (CR), b, made from 316 stainless steel with two sapphire viewing windows (front and back) to allow observation inside the reactor during the experiment. The crystallizer was designed to withstand up to 20 MPa and had an internal volume of 80 cm³. In addition, the 50 cm³ reservoir (R) was also connected to

both systems. Both crystallizer and reservoir were immersed in a cooling bath. An external refrigerator (ER) (Model RC-20, Labtech, India) circulating the water and glycol mixing in the ratio of 4:1 was used to maintain the temperature in the crystallizer. The pressure transmitter (PT) (Cole Pamer, Model 68,073, Singapore) was used to measure the pressure in the system with the range 0-21 MPa with the uncertainty of 0.13%. An analog pressure gauge (Swagelok, USA) was also used to monitor pressure in the system. The reactor temperature was measured by a K-type thermocouple (TC) (SL heater, Thailand) with a ± 0.5 K accuracy. The pressure and temperature during the experiment were recorded by a data logger (DL) (AI210, Wisco Industrial Instruments, Thailand), which was connected to a personal computer (PC). The temperature and pressure data were recorded every 10 seconds using a software provided by Wisco Industrial Instruments, Thailand. For morphology observation, the images and videos during hydrate formation and dissociation were captured by a camera (VC) (Optika, Model C-HP, Italy) with the macro camera lens (VS Technology Corporation, Japan). For the hybrid method, a magnetic stirrer bar was placed inside the crystallizer and was controlled by a magnetic stirrer.

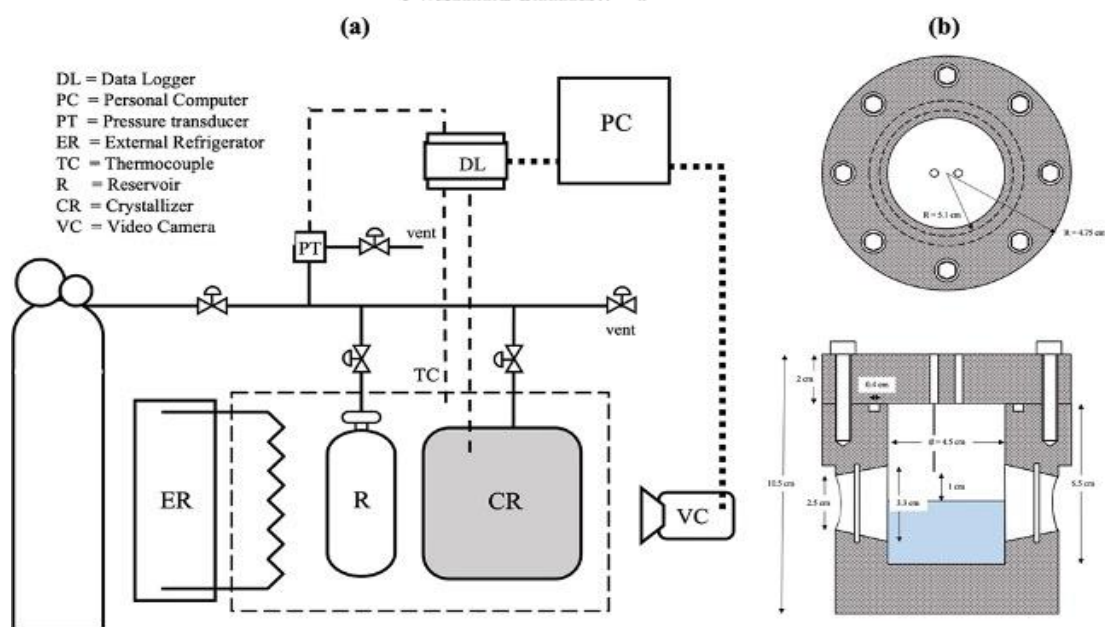


Figure 3.1 Schematic of (a) experimental apparatus and (b) cross-section of window crystallizer (modified from Siangsai *et al.* (2015)).

3.2.2 Hydrate Formation Experiment

All experiments were batch type for the observation of formation and dissociation of methane hydrates. 35 cm³, which was amino acid diluted with water, was placed into the window crystallizer. Then, the crystallizer was immersed in a cooling bath, and its temperature was controlled by using external refrigerator. The crystallizer was flushed three times with 0.5 MPa methane gas to remove air from the system. After the temperature inside the crystallizer reached the desired temperature (277.2 K), methane gas was introduced to the system at 8 MPa. 500 rpm stirring rate was started by the magnetic stirrer. After the hydration nucleation was observed, the stirring was stopped. During the hydrate formation, pressure and temperature were recorded every 10 seconds, until there was no further pressure drop for at least 1 hour. For morphology study, the images were captured every 10 seconds. The calculation procedure in this study was similar to the previous study by our group, Inkong *et al.* (2019a) and Siangsai *et al.* (2015). The pressure and temperature data were used to calculate the moles of methane consumed and methane gas uptake by Equation (3.1) and Equation (3.2), respectively

$$\Delta n_{H,\downarrow} = n_{H,0} - n_{H,t} = \left(\frac{PV}{zRT} \right)_{G,0} - \left(\frac{PV}{zRT} \right)_{G,t} \quad (3.1)$$

$$\text{Methane gas uptake} = \frac{(\Delta n_{H,\downarrow})_t}{n_{H_2O}} \quad (\text{mole of CH}_4/\text{mole H}_2\text{O}) \quad (3.2)$$

where

- $\Delta n_{H,\downarrow}$ = moles of consumed gas for hydrate formation (mole),
- $n_{H,t}$ = moles of methane gas at time t (mole),
- $n_{H,0}$ = moles of methane gas at time 0 (mole),
- P = pressure of the crystallizer (atm),
- T = temperature of the crystallizer (K),
- V = the volume of gas phase in the crystallizer (cm³),
- Z = compressibility factor Pitzer's correlation, and
- R = the universal gas constant 82.06 cm³•atm/mol•K,

The water to hydrate conversion was calculated from Equation (3.3), as follows (Linga *et al.*, 2010)

$$\text{Conversion (\%)} = \frac{\Delta n_{H,\uparrow} \times \text{Hydration number}}{n_{H_2O}} \times 100 \quad (3.3)$$

The hydration number is the number of water molecules required to form the hydrate structure per gas molecule. This number is determined to be 5.75 for the sI hydrate structure formed in our experiments (Inkong *et al.*, 2019c). The hydrate formation rate was represented by the normalized initial hydrate formation rate for the first 30 minutes after hydrate nucleation (NR_{30}) and was calculated by Equation (3.4).

$$NR_{30} = \frac{R_{30}}{V_{\text{water}}} \quad (3.4)$$

where V_{water} is the volume of water (m^3) taken in the reactor, and R_{30} is the rate of hydrate growth (kmol/hr) calculated by fitting the gas uptake due to the hydrate growth at each experimental condition versus time for the first 30 minutes after the induction time.

3.2.3 Hydrate Dissociation Experiment

After the completion of methane hydrate formation, methane hydrates were dissociated through thermal stimulation by increasing the temperature to 298.2 K. The start of the temperature rise is considered as time zero for the hydrate dissociation experiments. The gas released from the gas hydrates was measured by the pressure transducer. The experiment was stopped when the pressure in the reactor remained constant at the experimental temperature (298.2 K). The number of moles of methane gas released from the hydrates during the dissociation experiment at given any time (t) was calculated by Equation (3.5).

$$\Delta n_{H,\uparrow} = n_{H,t} - n_{H,0} = \left(\frac{PV}{zRT} \right)_{G,t} - \left(\frac{PV}{zRT} \right)_{G,0} \quad (3.5)$$

This equation is the negative of Equation (3.1) detailed above, as it begins with fewer moles of gas and increases in the moles as the dissociation progresses. The methane recovery was calculated by Equation (3.6) (Babu *et al.*, 2013; Linga *et al.*, 2009).

$$\% \text{ Methane recovery} = \frac{(\Delta n_{H,\uparrow})_t}{(\Delta n_{H,\downarrow})_{end}} \times 100 \quad (3.6)$$

where $\Delta n_{H,\uparrow}$ is moles of released gas from hydrates during the hydrate dissociation at any given time. And $(\Delta n_{H,\downarrow})_{End}$ is moles of gas consumption for hydrate formation at the end of experiments.



CHAPTER 4

RESULT AND DISCUSSION

This work investigated the effects of different amino acids on methane hydrate formation and dissociation in terms of kinetics and morphology. Three amino acids, including L-valine, L-leucine, and L-methionine were investigated at the concentration of 0.25, 0.50, and 1.00 wt%, which is in the range used in the previous studies in our group (Inkong *et al.*, 2022b; Jeenuang *et al.*, 2021). The chemical structures of investigated amino acids are presented in Figure 4.1.

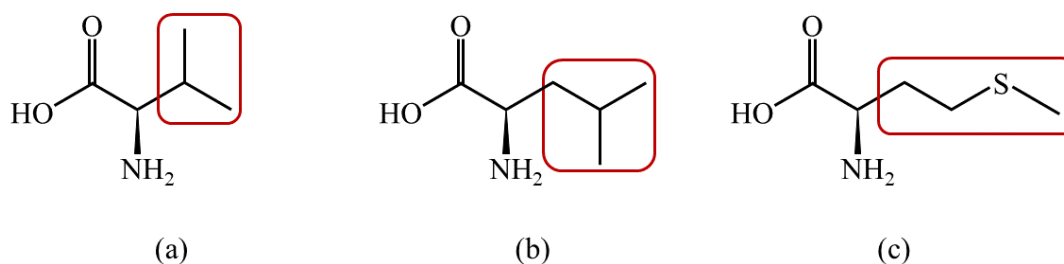


Figure 4.1 Structure of nonpolar amino acids (a) L-valine, (b) L-leucine, and (c) L-methionine.

The formation conditions were 8 MPa and 277.2 K, this condition is in the SI region of pure methane hydrate phase equilibrium (Sloan Jr and Koh, 2007). Firstly, methane hydrate formation using 1.00 wt% of each amino acid was performed in an unstirred reactor system. However, the methane hydrate formation cannot be observed, even though the experimental conditions performed at the high driving forces about 4.09 MPa pressure driving force and 6.96 K temperature driving force, which is sufficient for the formation (Nakamura *et al.*, 2003) and the presence of the amino acids. Therefore, the experimental formation conditions and the hydrate promoter applied in this work are not the restraint to form the hydrate formation in this work. Another key point to promote the hydrate formation is the increase in the surface contact area by the reactor design. Firstly, this work is performed using the unstirred reactor, which has low surface contact area between the two phases. Therefore, the lower amount of methane gas molecules dissolve into the liquid phase,

which may not be enough for hydrate nucleation. To overcome the limitation of the reactor design, the HCR approach was applied in this work. The procedure of HCR approach is divided into two steps. The methane hydrate formation is first conducted in a stirred reactor to induce the hydrate nucleation. The stirring increases the surface contact area between the two phases to enhance the gas dissolution into the liquid phase. Then, the stirring is stopped, and the hydrate growth is allowed to continue in an unstirred reactor, taking an advantage of kinetic promoting activity of amino acids (Bhattacharjee and Linga, 2021; Veluswamy *et al.*, 2017a). Three experiments at each amino acid concentration were conducted to ensure repeatability. From the experiments, it was found that using the HCR approach can induce methane hydrate formation at 8 MPa and 277.2 K, even in the system with low amino acid concentrations.

4.1 Effect of L-valine on Methane Hydrate Formation

First, the methane hydrate formation in the presence of L-valine was performed to study the effects of L-valine concentration on the kinetics of methane hydrate formation in the HCR approach. Table 4.1 presents the details on induction time, normalized rate of hydrate formation (NR_{30}), time required to reach 90% of final methane uptake calculated from the nucleation (t_{90}), methane uptake, water to hydrate conversion, and methane recovery in various concentrations of L-valine solution at 8 MPa and 277.2 K. It can be observed from the table that L-valine can promote hydrate formation at all concentrations in the HCR approach. It can be confirmed that the HCR approach can enhance the increase in the surface contact area between the two phases, resulting in the increased mass transport of the gas molecules into the liquid phase.

Table 4.1 Experimental results for methane hydrate formation using different L-valine concentrations at 8 MPa and 277.2 K

Amino acid conc. (wt%)	No. Exp.	^a Induction time (min)	^b NR ₃₀ (kmol of gas/ m ³ of water/hr)	^c t ₉₀ (min)	Methane uptake (mmol of gas/ mol of water)	Water to hydrate conversion (%)	% Methane recovery
0.25	A1	56.47	0.44	198.83	122.91	70.68	97.30
	A2	49.97	0.51	208.33	129.50	74.46	99.69
	A3	54.03	0.42	204.50	136.13	78.28	98.43
0.50	B1	49.07	1.48	138.17	133.15	76.56	97.24
	B2	53.90	1.59	167.00	145.00	83.38	98.42
	B3	47.30	1.64	128.33	133.15	76.56	97.24
1.00	C1	26.53	2.64	95.50	138.70	79.75	98.85
	C2	34.20	2.15	87.00	143.74	79.58	98.84
	C3	28.17	2.48	75.50	134.31	79.75	96.47

^a Induction time is the time interval between the starting point of the experiment (the stirring started) and the nucleation of the first hydrate crystal (the stirring stopped).

^b NR₃₀ is the normalized rate of hydrate formation 30 min from the induction time.

^c t₉₀ is the time required to reach 90% of the final methane uptake calculated from the nucleation.

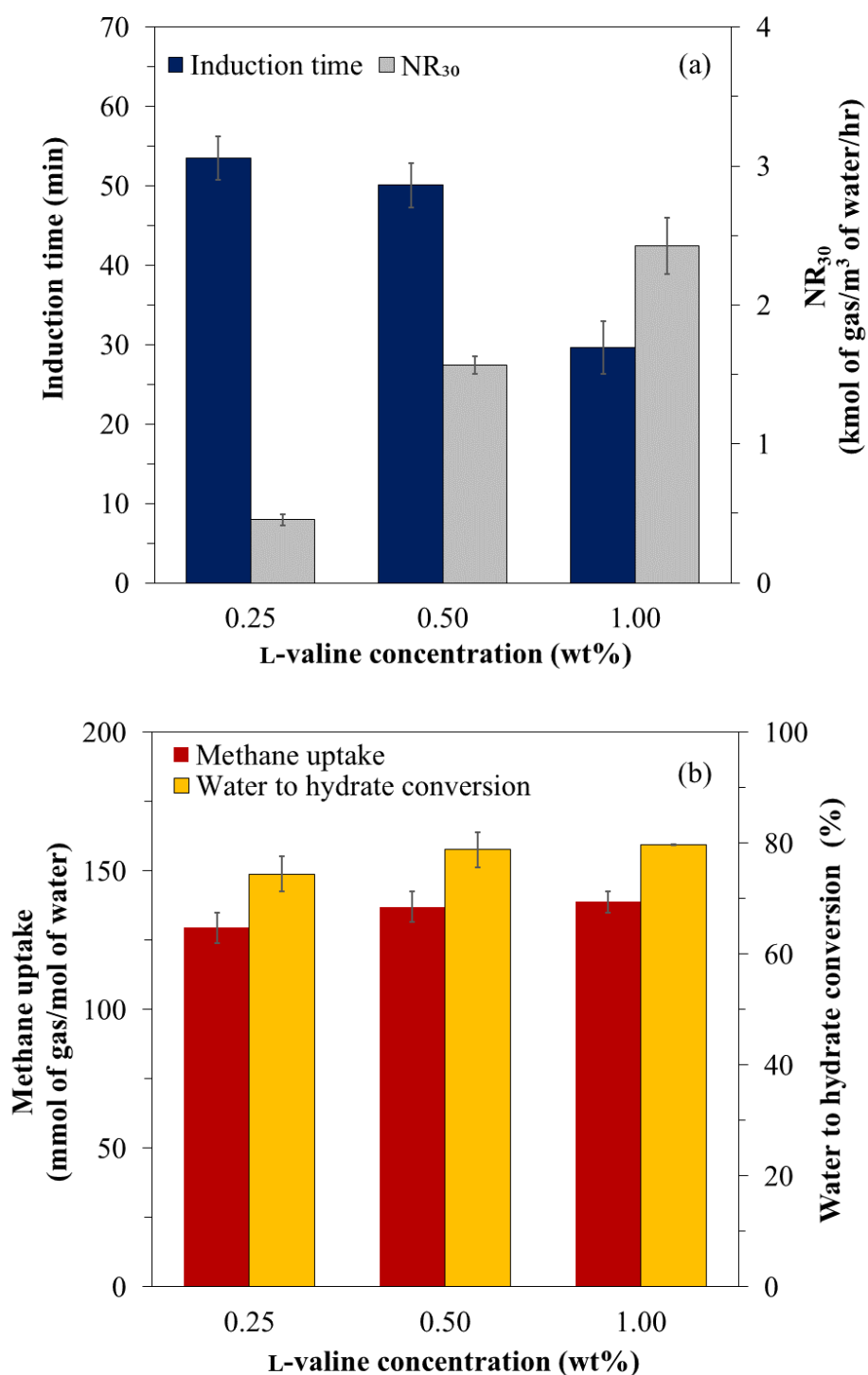


Figure 4.2 Effects of L-valine concentrations on (a) induction time and NR_{30} and (b) methane uptake and water to hydrate conversion on methane hydrate formation at 8 MPa and 277.2 K.

Figure 4.2a shows the induction time and the rate of hydrate formation in the presence of different L-valine concentrations, using the data in Table 4.1. The induction times are comparable at 0.25 and 0.50 wt% L-valine solutions, which lasted at least 50 minutes, but significantly decrease at 1.00 wt% L-valine solution. In addition, the rate of hydrate formation (NR_{30}) increases as the L-valine concentration increases. This is because the presence of amino acids decreases the interfacial surface tension between the gas and liquid phases, promoting gas molecules to easily transport into the liquid phase for hydrates to nucleate (Raza *et al.*, 2019). Moreover, the interfacial surface tension decreases along with the increase in the amino acid concentration (Belton and Twidle, 1940). However, the final methane uptake and the water to hydrate conversion are the same in all L-valine concentrations, as shown in Figure 4.2b. The results are consistent with the literature that an amino acid served only as a kinetic promoter for hydrate formation without changing the final gas uptake (Cai *et al.*, 2017; Inkong *et al.*, 2022b; Liu *et al.*, 2015).

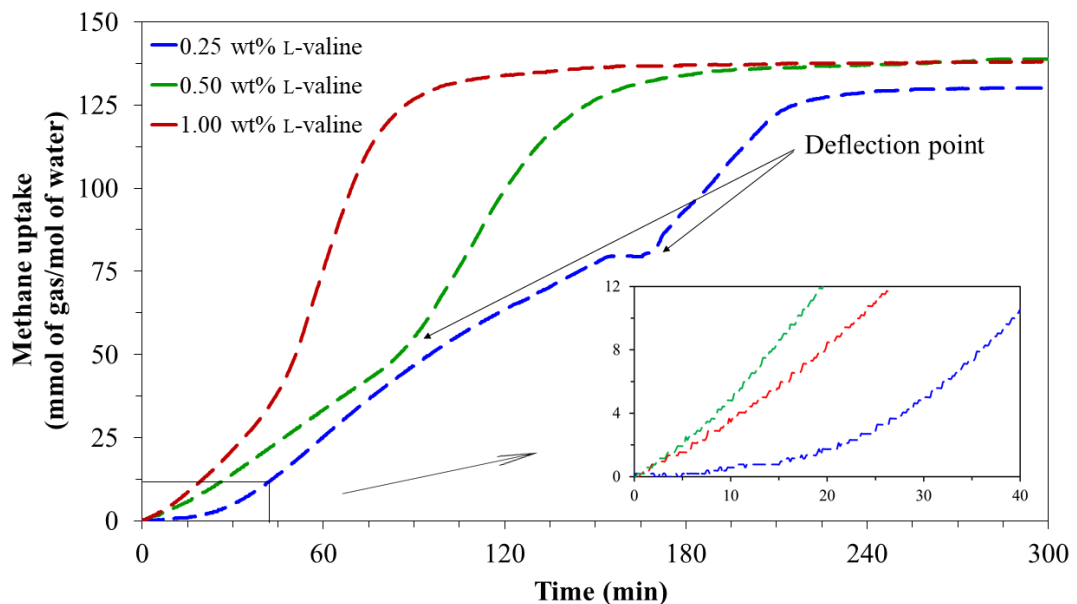


Figure 4.3 Average methane uptake profiles during methane hydrate formation using different concentrations of L-valine at 8 MPa and 277.2 K.

Furthermore, the average methane uptake profiles during methane hydrate formation at three different L-valine concentrations are shown in Figure 4.3. With

0.25 wt% L-valine solution, a short deflection can be observed at the beginning of the hydrate formation around 0-30 minutes, resulting in the low hydrate formation rate. Interestingly, there is a change in the slope of the gas uptake between 160 and 180 minutes. This can be explained by the immobile transitional states of water, which cause the gas uptake to always lag after the disappearance of liquid water and the formation of solid hydrates at the area of hydrate formation, as described in literature (Botimer *et al.*, 2016; Veluswamy *et al.*, 2016a). In addition, the hydrate formation takes about 203.89 (± 3.90) minutes to complete 90% of the final methane uptake (t_{90}), and the final methane uptake is low, Table 4.1. The increase in the L-valine concentration to 0.50 wt% results in significantly faster hydrate formation. Although the induction time is close to 0.25 wt% L-valine solution, the t_{90} value is significantly lower. Intriguingly, deflection points of multiple-stage methane hydrate formation are observed in both 0.25 and 0.50 wt% L-valine solutions. This characteristic has been demonstrated in many studies. The cause of the deflection point is that the hydrate formation gradually progresses with the use of low doses of L-valine (0.25 and 0.50 wt%). The growth of hydrates blocks and reduces the surface contact area. Gas consumption is reduced, causing the deflection point. Later, the hydrates are cracked and the free gas is consumed for further formation, leading to multi-stage hydrate growth (Inkong *et al.*, 2019b; Inkong *et al.*, 2019c; Siangsai *et al.*, 2018; Siangsai *et al.*, 2015). The increase in the L-valine concentration to 1.00 wt% enhances the hydrate formation kinetics, whereby both induction time and t_{90} decrease. This is due to the decrease in the mass transfer resistance with the increase in the L-valine concentration (Ohmura *et al.*, 2005). On the contrary, the hydrate growth occurs in a single stage in the 1.00 wt% L-valine solution, unlike the 0.25 and 0.50 wt% L-valine solutions. The methane hydrate kinetic promotion behavior of L-valine is similar to that of surfactants (Liu *et al.*, 2015; Veluswamy *et al.*, 2017b). The key role of L-valine and surfactants is to decrease the interfacial surface tension between the gas and liquid phases. The surface tension values of amino acids are demonstrated in the literature (Gliński *et al.*, 2000; Raza *et al.*, 2019; Rodríguez and Romero, 2017). The decrease in the interface surface tension between the gas and liquid phases improves the mass transfer coefficient, resulting in gas molecules to easily diffuse into the liquid phase and aid in hydrate nucleation and hydrate growth (Kumar *et al.*, 2015;

Raza *et al.*, 2019; Rodríguez and Romero, 2017; Sun *et al.*, 2018). Additionally, L-valine may inhibit the aggregation of hydrates at the gas-liquid interface during the hydrate formation. This allows more methane to enter the liquid phase, hence increasing the amount of methane in the formation (Partoon *et al.*, 2013). This mechanism is supported by the visual morphology observations during methane hydrate formation, which will be described next. However, the decrease in the surface tension of surfactant is better than that of amino acid; therefore, the presence of surfactant can promote methane hydrate formation even with low concentrations (Inkong *et al.*, 2019c; Siangsai *et al.*, 2018; Wang *et al.*, 2015).

In terms of morphology, images were taken every 10 seconds during the hydrate formation using a camera through a sapphire window. All experiments were conducted at the same condition of 8 MPa and 277.2 K. Figure 4.4 depicts visual observations of methane hydrate formation at various time intervals in the presence of L-valine concentrations. It can be seen that the hydrates first occur at the vortex interface. This area provides a large surface contact area between the gas and liquid phases, resulting in the hydrate nucleation at this area. Then, the methane hydrates simultaneously grow upward into the gas phase along the reactor wall. This is because the water molecules from the solution are transported upward into the gas phase via the capillary channel between hydrate crystals (Bhattacharjee *et al.*, 2020; Bhattacharjee and Linga, 2021; Veluswamy *et al.*, 2016a). Thus, the water molecules transported from the solution easily contact methane gas in the gas phase, resulting in the conversion to methane hydrates. Next, the methane hydrates grow downward into the bulk solution. With 0.25 wt% L-valine solution, the hydrate growth occurs gradually above the gas-liquid interface. This corresponds to the methane uptake profiles of 0.25 and 0.50 wt% L-valine systems, where deflections are observed between 160 and 180 minutes, Figure 4.3. Following this, the hydrates grow rapidly both above and below the gas-liquid interface. However, the hydrates cannot form to cover the entire window at the end of hydrate formation process, which may be the result of the immobile transitional states of water and an insufficient amount of L-valine to promote the hydrate formation, as described earlier. With 0.50 wt% L-valine solution, the hydrates grow continuously in both directions and almost cover the entire window at the end of the process. In the case of 1.00 wt% L-valine, the rapid

growth of hydrates after hydrate nucleation in both directions is significantly faster than in the 0.25 and 0.50 wt% L-valine systems. Within 120 minutes, the hydrates completely cover the entire window. This corresponds to the methane uptake profiles in Figure 4.3.

Interestingly, after the hydrate nucleation at the interface, the characteristics of the hydrate formation using L-valine at different concentrations are shown in Figure 4.5. It shows the zoomed morphological observations of methane hydrate formation in the presence of L-valine after hydrate nucleation. It can be clearly observed that the hydrate crystals form and float in the bulk solution, Figures 4.5a and 4.5c. This is because of the inertia force of the solution, which results in the movement of the solution even after the stirring is stopped. Hydrate crystals are pulled down and dispersed in the bulk solution. Later, the hydrate crystals gradually float to the surface due to the buoyancy force. Furthermore, the capillary channels can be observed during the hydrate growth, Figures 4.5a and 4.5e. This is a characteristic of the porous hydrate structure. The bulk aqueous solution is carried through the porous hydrate structure via the capillary channels to the surface of the already formed hydrate layer and into contact with the existing methane gas, allowing further hydrate growth in the upward direction (Bhattacharjee and Linga, 2021). The characteristic of capillary channel was also reported by Veluswamy *et al.* (2016c), who investigated the mixed methane-THF hydrate formation using THF solution. Moreover, the characteristic methane bubble formation is observed in all L-valine experiments, Figures 4.5b, 4.5d, and 4.5f. The methane bubbles eventually expand in size and the hydrates become dense. This developing bubble hydrate layer links with the primary hydrate layer that allows gas molecules to interact with the bulk solution, resulting in more hydrate formation. This characteristic growth is consistent with an investigation of the morphology during methane hydrate formation and dissociation by Veluswamy *et al.* (2016a). Moreover, it can be seen that the L-valine concentrations have no effect on the pattern of methane hydrate formation.

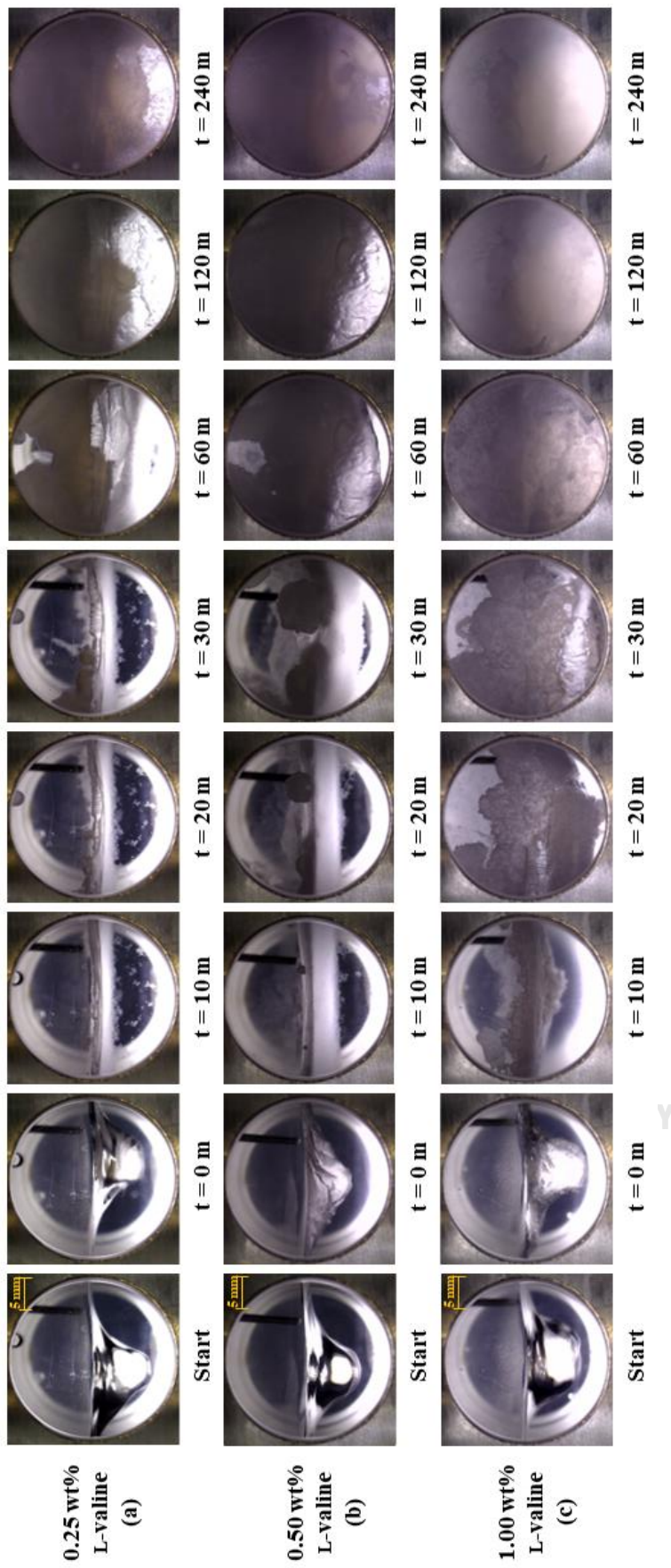


Figure 4.4 Morphology observation during methane hydrate formation using different L-valine concentrations at 8 MPa and 277.2 K.

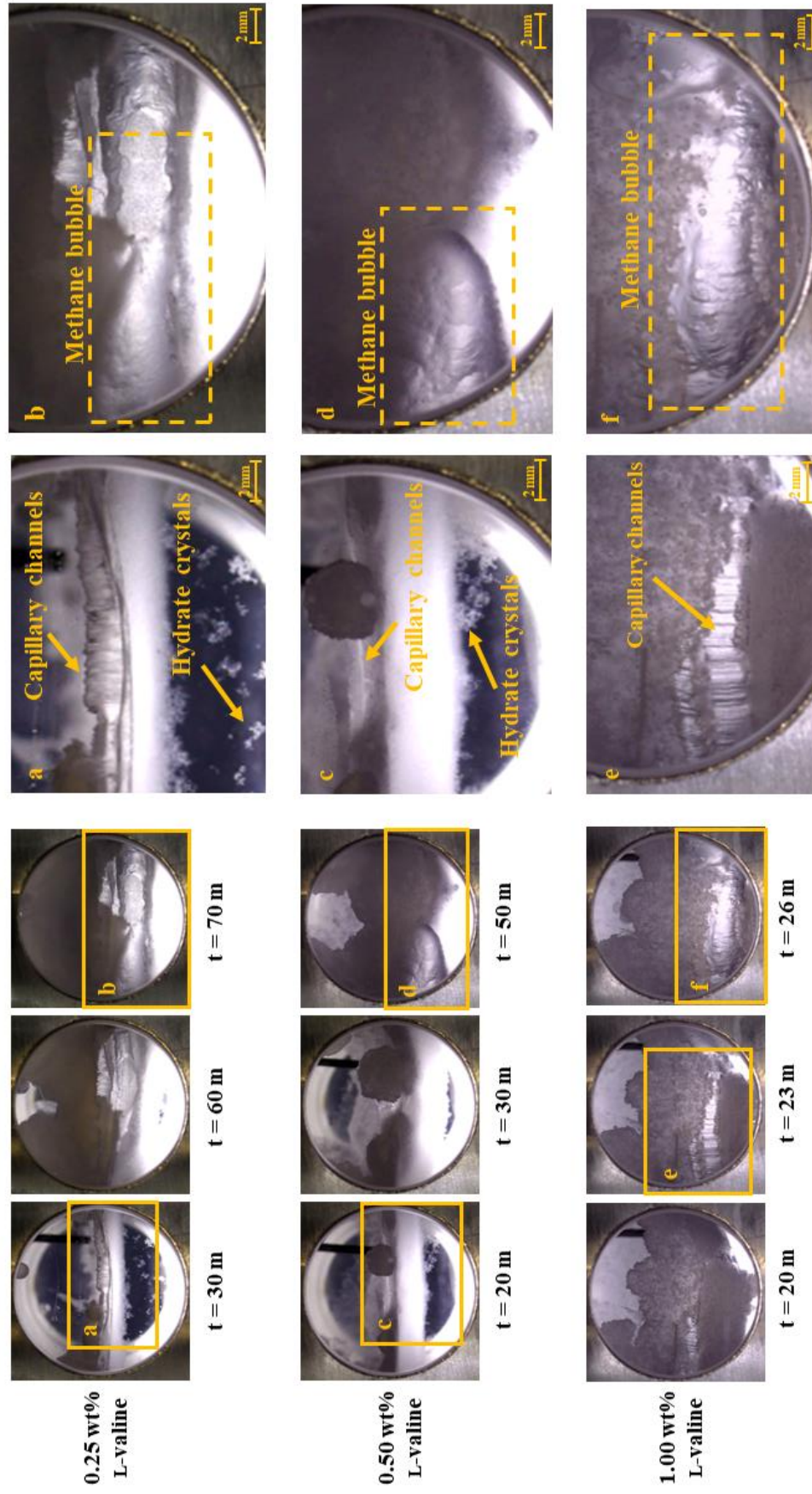


Figure 4.5 Zoomed morphology of methane hydrate formation in the presence of L-valine.

4.2 Effect of L-leucine on Methane Hydrate Formation

The next set of experiments investigate the effect of L-leucine at various concentrations (0.25, 0.50, and 1.00 wt%) was investigated. The methane hydrate formation in the presence of L-leucine was performed at 8 MPa and 277.2 K using the HCR approach. L-leucine has been widely reported to be an amino acid that significantly promotes the kinetics of methane hydrate formation (Liu *et al.*, 2015; Veluswamy *et al.*, 2016a; Veluswamy *et al.*, 2017a). Table 4.2 presents induction time, rate of hydrate formation (NR_{30}), time required to reach 90% of final methane uptake calculated from the nucleation (t_{90}), methane uptake, water to hydrate conversion, and methane recovery for all experiments using various concentrations of L-leucine solution. Interestingly, it can be observed from Table 4.2 that L-leucine effectively promotes the methane hydrate formation at all concentrations using the HCR approach.

Figure 4.6a presents the induction time and the rate of hydrate formation in the presence of L-leucine concentrations. It can be seen that the induction time of the presence of 0.25 and 0.50 wt% L-leucine solution gives very similar results, which are 23.02 (± 1.01) and 23.42 (± 0.69) minutes, respectively. With the increase in the L-leucine concentration to 1.00 wt%, the induction time decreases to 18.51 (± 1.33) minutes. However, it is possible that the 0.50 wt% L-leucine system takes a longer time than the 0.25 wt% L-leucine system because of the stochastic nature of hydrate formation. In terms of hydrate formation rate (NR_{30}), the results are similar at 0.25 and 0.50 wt% L-leucine solutions, but significantly increase with the increase in the L-leucine concentration to 1.00 wt%. In the same way as L-valine, L-leucine can promote methane hydrate formation by decreasing the gas-liquid interfacial tension, which allows gas molecules to easily enter the liquid phase and convert to hydrates. Also, the interfacial surface tension decreases as the L-leucine concentration increases. However, the final methane uptake and the water to hydrate conversion are the same in all L-leucine concentrations, as shown in Figure 4.6b. Moreover, they are also similar to those of L-valine systems, as mentioned earlier.

Table 4.2 Experimental results for methane hydrate formation using different L-leucine concentrations at 8 MPa and 277.2 K

Amino acid conc. (wt%) ⁱ	No. Exp.	^a Induction time (min)	^b NR ₃₀ (kmol of gas/ m ³ of water/hr)	^c t ₉₀ (min)	Methane uptake (mmol of gas/ mol of water)	Water to hydrate conversion (%)	% Methane recovery
0.25	D1	24.17	3.28	249.33	132.49	76.18	97.48
	D2	21.70	3.63	92.67	132.93	76.43	97.71
	D3	23.20	3.36	127.17	132.04	75.92	98.51
0.50	E1	22.73	3.76	67.33	136.29	78.37	97.84
	E2	23.17	3.97	81.67	133.77	76.92	97.30
	E3	24.37	3.50	94.50	132.75	76.33	97.38
1.00	F1	16.63	5.38	55.83	131.30	73.14	95.89
	F2	19.53	5.75	52.67	130.56	75.07	95.92
	F3	19.37	5.57	55.50	130.68	72.79	97.28

^a Induction time is the time interval between the starting point of the experiment (the stirring started) and the nucleation of the first hydrate crystal (the stirring stopped).

^b NR₃₀ is the normalized rate of hydrate formation 30 min from the induction time.

^c t₉₀ is the time required to reach 90% of the final methane uptake calculated from the nucleation.

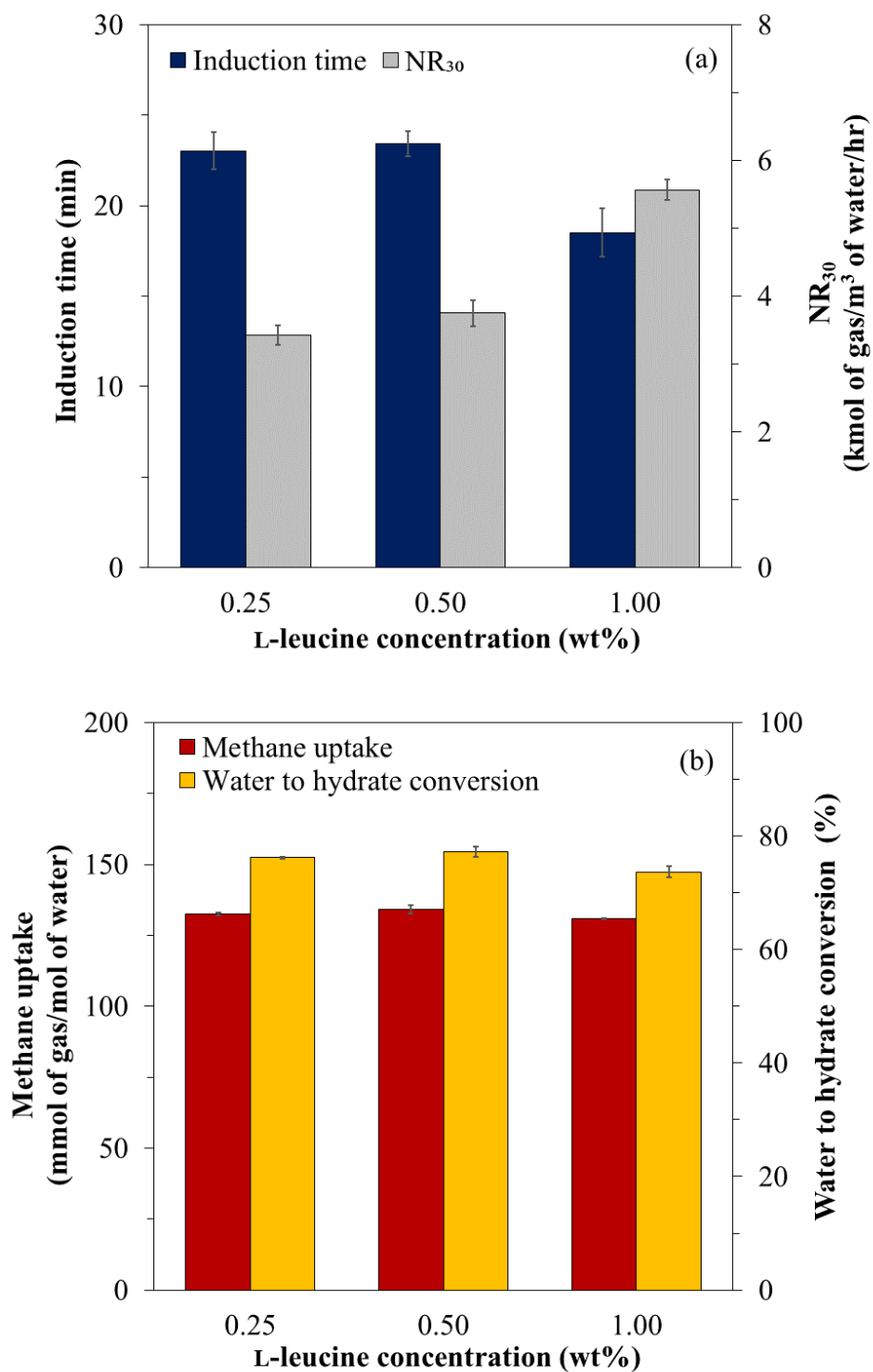


Figure 4.6 Effects of L-leucine concentrations on (a) induction time and NR_{30} and (b) methane uptake and water to hydrate conversion on methane hydrate formation at 8 MPa and 277.2 K.

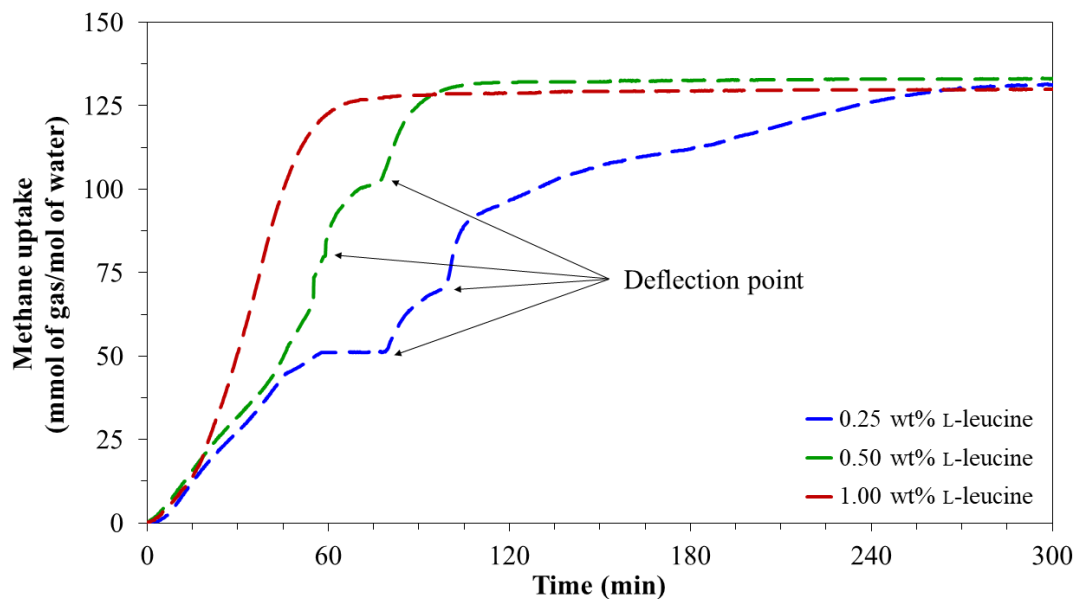


Figure 4.7 Average methane uptake profiles during methane hydrate formation using different L-leucine concentration at 8 MPa and 277.2 K.

Figure 4.7 presents the average methane uptake profiles during methane hydrate formation at three different L-leucine concentrations. With 0.25 and 0.50 wt% L-leucine solutions, the hydrates grow at the same rate (0-30 minutes after nucleation). The hydrate formation takes about 160 minutes to complete 90% of the final methane uptake (t_{90}) using a 0.25 wt% L-leucine solution. Upon increasing the L-leucine concentration to 0.50 wt%, it results in much faster hydrate formation. In addition, the multiple growth stages are also observed in both 0.25 and 0.50 wt% L-leucine solutions. This can be explained by the immobile transitional states of water at the low L-leucine concentrations, as discussed earlier. Interestingly, at the 1.00 wt% L-leucine solution, the methane hydrate growth occurs in a single stage with a high rate of hydrate formation, and the time taken for 90% completion of hydrate formation (t_{90}) is also reduced to 54.67 (± 1.42) minutes. The final methane uptakes are not significantly different at each L-leucine concentration. Additionally, methane uptake profiles are identical to those discussed in the L-valine system and also consistent with literatures (Veluswamy *et al.*, 2016a; Veluswamy *et al.*, 2017a).

The visual morphology observations of methane hydrate formation at different time intervals with various L-leucine concentrations are presented in Figure 4.8. At the

hydrate nucleation ($t = 0$ min), it can be observed that the solutions are turbid due to the hydrate nucleation occurring as the hydrate crystals along the gas-liquid interface, where the surface area is increased by stirring. These hydrate crystals are dispersed in the bulk solution by the solution movement after the stirring stops, resulting in turbidity of solution. Then, there is a rapid growth of hydrates in the downward direction into the bulk solution, which results in a cloudier solution as well as a slight growth of hydrates in the upward direction along the reactor wall. Following this, progressive hydrate formation takes place above the gas-liquid interface. Additionally, Figure 8 shows the zoomed morphological observations of methane hydrate formation in the presence of L-leucine. Figures 8a and 8d show the hydrate crystals dispersed in the bulk solution forming spontaneously porous hydrates. Similar to the discussion on the presence of L-valine, the capillary channels, which are the characteristic of a porous hydrate structure, can be clearly observed during the hydrate growth, Figure 8b. However, it can be noted that the distinct capillary channel of the hydrate development is present in a short time (Veluswamy *et al.*, 2016c). Therefore, it is unable to see the capillary channels at all concentrations. The hydrate crystals above the interface continue to grow up along the reactor wall until the hydrates form to cover the entire windows even at the low L-leucine concentrations (0.25 wt%), but it is observed that the hydrate structures grow loosely in the 0.25 wt% L-leucine system. With further increase in the L-leucine concentration, the hydrates grow faster and densely cover the entire window. The morphology during the methane hydrate formation in the presence of L-leucine in this work is consistent with the morphology study of methane hydrate formation in the presence of amino acid by Veluswamy *et al.* (2016a).

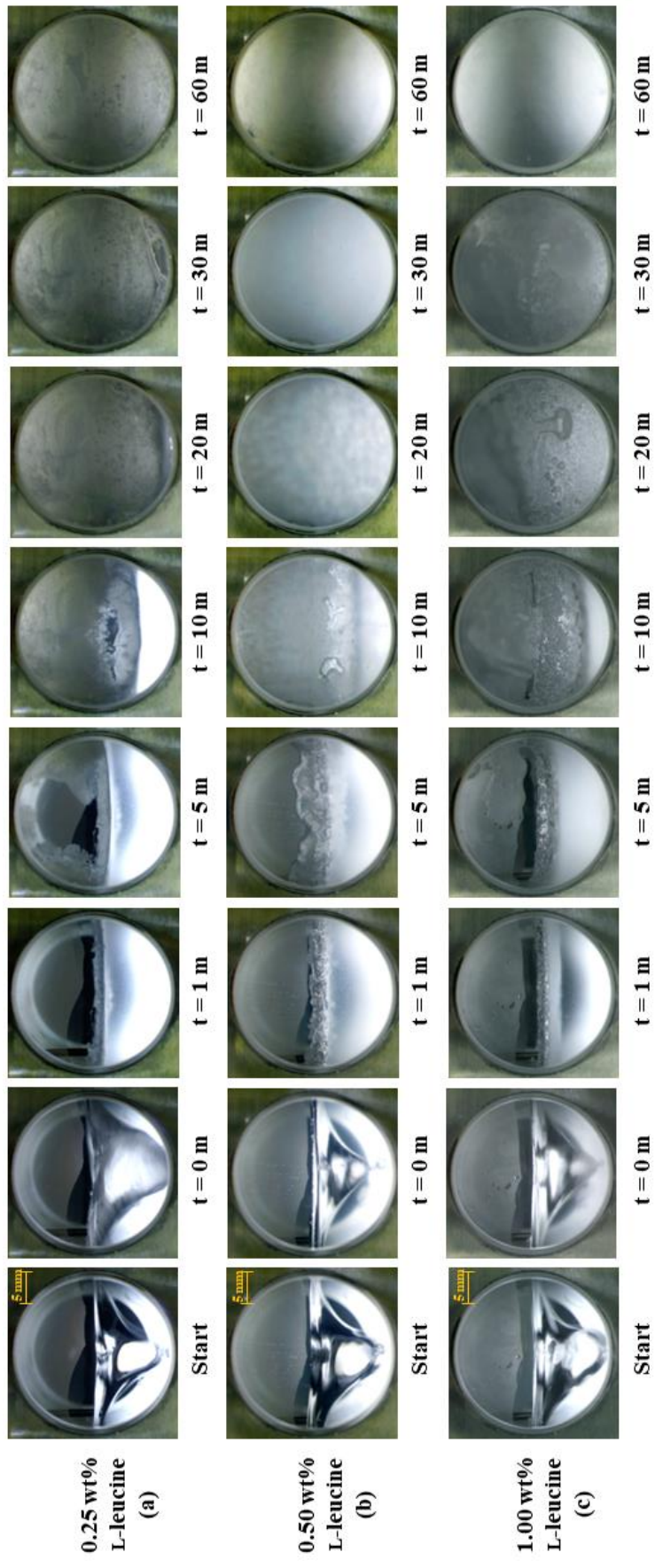


Figure 4.8 Morphology observation during methane hydrate formation using different L-leucine concentrations at 8 MPa and 277.2 K.

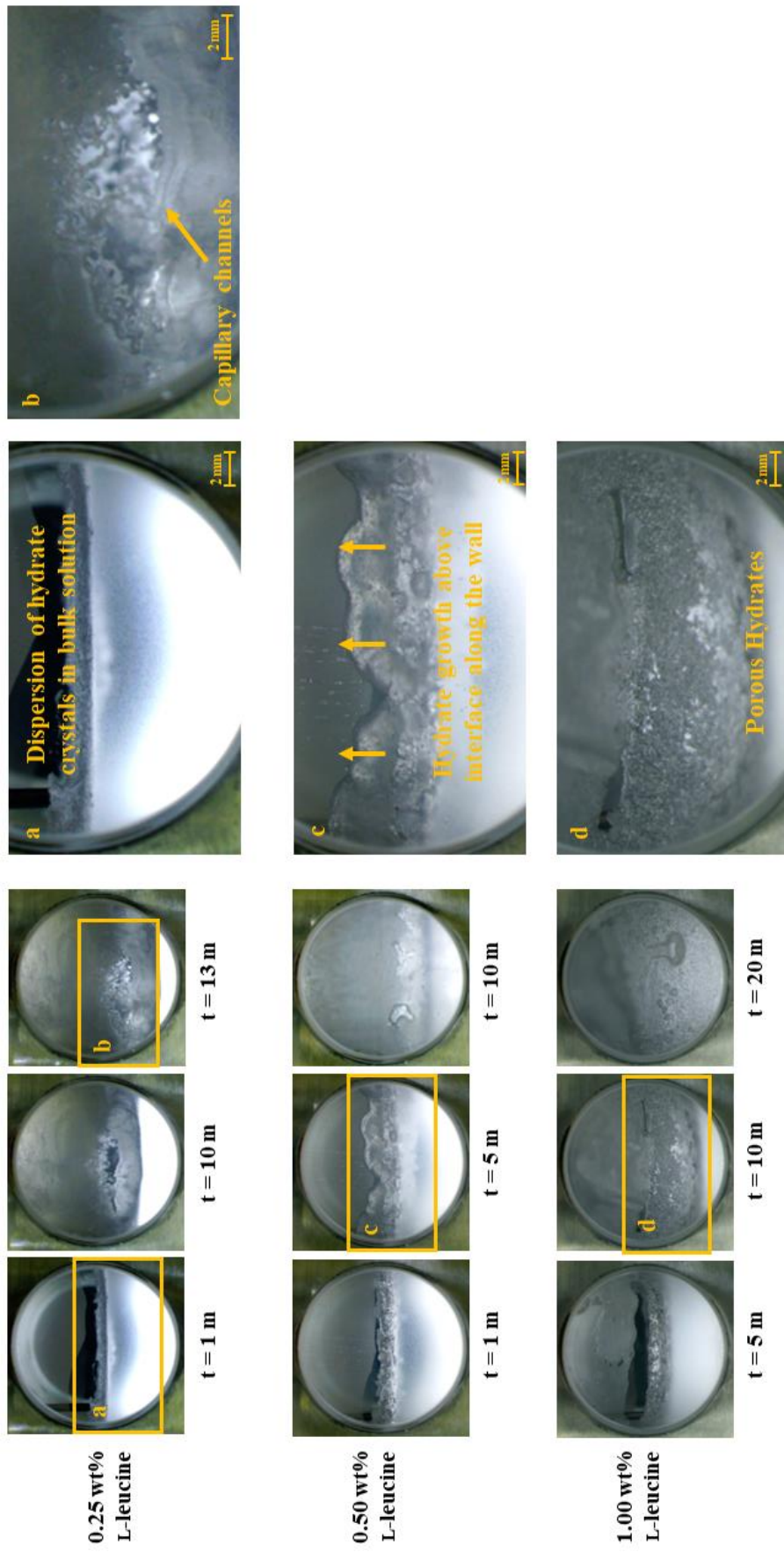


Figure 4.9 Zoomed morphology of methane hydrate formation in the presence of L-leucine.

4.3 Effect of L-methionine on Methane Hydrate Formation

The formation of methane hydrates in the presence of L-methionine was carried out at 8 MPa and 277.2 K using the HCR approach. Table 4.3 summarizes the methane hydrate formation kinetic parameters; the induction time, the rate of hydrate formation (NR_{30}), the time required to reach 90% of final methane uptake calculated from the nucleation (t_{90}), the methane uptake, the water to hydrate conversion, and the methane recovery for all experiments using various L-methionine concentrations of 0.25, 0.50, and 1.00 wt%.

The induction time and the rate of hydrate formation in the presence of L-valine concentrations are depicted in Figure 4.10a. The induction time is identical to that of the L-leucine system, as discussed in the previous section. The L-methionine induction time seems to be higher with 0.50 wt% L-methionine than 0.25 wt% L-methionine. Although this may seem to go against the expected trend, the stochastic nature of hydrate induction time measurement is a reasonable explanation (Inkong *et al.*, 2022a). Additionally, the NR_{30} significantly increases as the L-methionine concentration increases. An interesting observation is that when the L-methionine concentration is increased to 1.00 wt%, it can promote methane hydrate formation with the highest rate of 12.28 (± 0.22) kmol of gas/hr/m³ of water. L-methionine also exhibits an effect on methane hydrate formation kinetics similar to L-valine and L-leucine by reducing the gas-liquid interfacial tension. Moreover, L-methionine may act as a dispersant to prevent the agglomeration of hydrate particles and the formation of a hydrate film at the gas-liquid interface, which would inhibit further hydrate formation (Cai *et al.*, 2017; Uchida *et al.*, 1999). Figure 4.10b shows the final methane uptake and the water to hydrate conversion using different L-methionine concentrations. Similarly, there is no effect of L-methionine concentration on the final methane uptake and the water to hydrate conversion as demonstrated in all experiments.

Table 4.3 Experimental results for methane hydrate formation using different L-leucine concentrations at 8 MPa and 277.2 K

Amino acid conc. (wt%)	No. Exp.	^a Induction time (min)	^b NR ₃₀ (kmol of gas/ m ³ of water/hr)	^c t ₉₀ (min)	Methane uptake (mmol of gas/ mol of water)	Water to hydrate conversion (%)	% Methane recovery
0.25	D1	24.17	3.28	249.33	132.49	76.18	97.48
	D2	21.70	3.63	92.67	132.93	76.43	97.71
	D3	23.20	3.36	127.17	132.04	75.92	98.51
0.50	E1	22.73	3.76	67.33	136.29	78.37	97.84
	E2	23.17	3.97	81.67	133.77	76.92	97.30
	E3	24.37	3.50	94.50	132.75	76.33	97.38
1.00	F1	16.63	5.38	55.83	131.30	73.14	95.89
	F2	19.53	5.75	52.67	130.56	75.07	95.92
	F3	19.37	5.57	55.50	130.68	72.79	97.28

^a Induction time is the time interval between the starting point of the experiment (the stirring started) and the nucleation of the first hydrate crystal (the stirring stopped).

^b NR₃₀ is the normalized rate of hydrate formation 30 min from the induction time.

^c t₉₀ is the time required to reach 90% of the final methane uptake calculated from the nucleation.

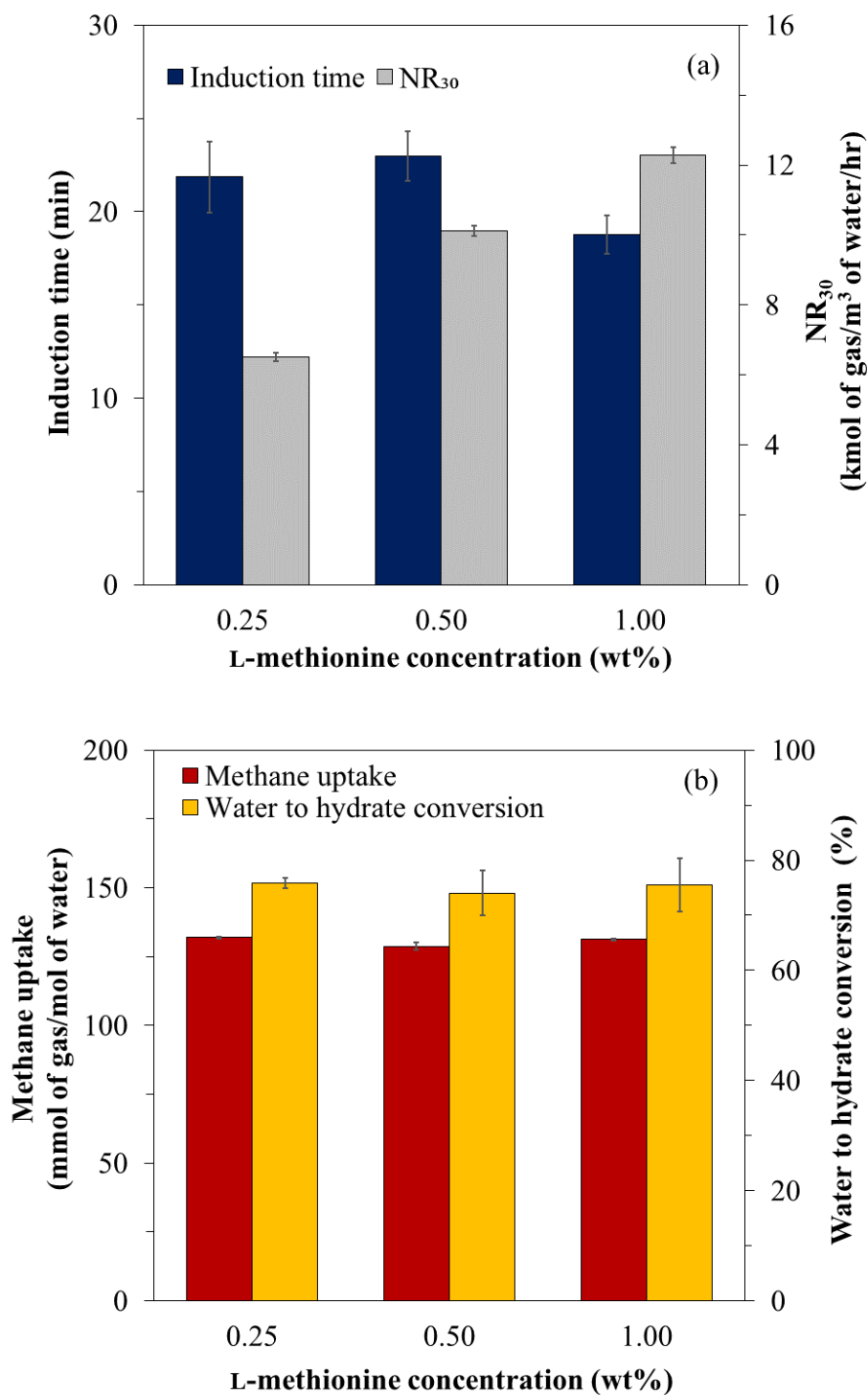


Figure 4.10 Effects of L-methionine concentrations on (a) induction time and NR_{30} and (b) methane uptake and water to hydrate conversion on methane hydrate formation at 8 MPa and 277.2 K.

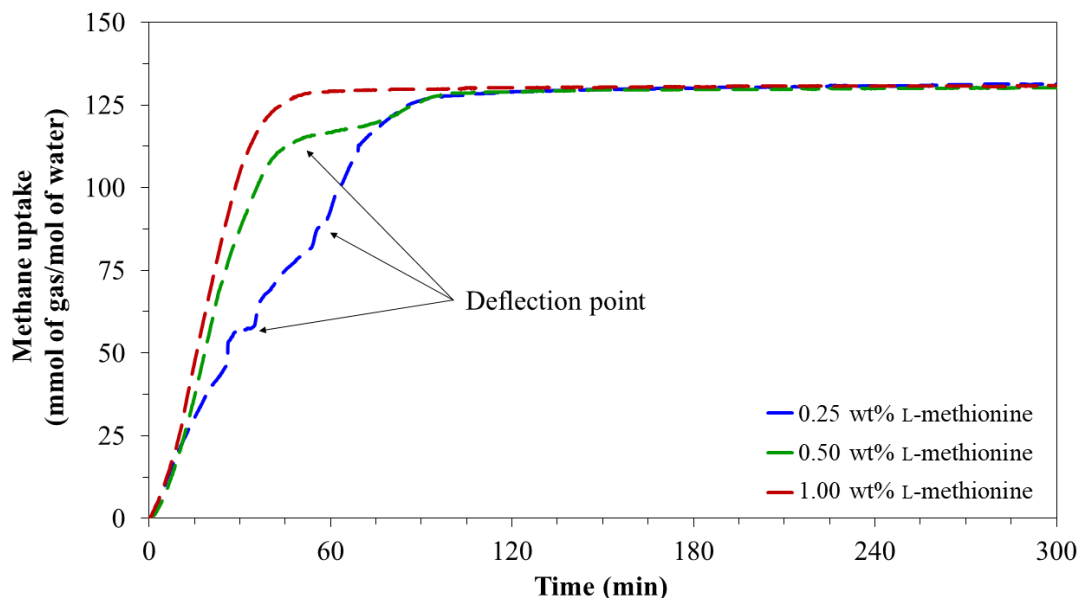
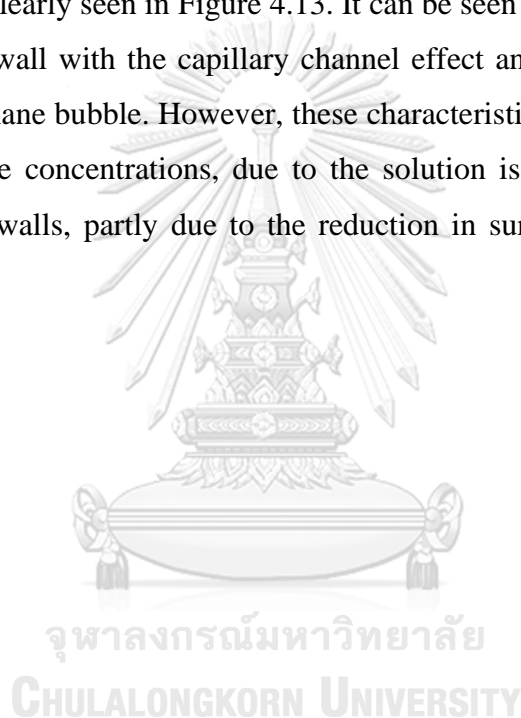


Figure 4.11 Average methane uptake profiles during methane hydrate formation using different L-methionine concentration at 8 MPa and 277.2 K.

Figure 4.11 presents the average methane uptake profiles during methane hydrate formation with three different L-methionine concentrations. At 0-30 minutes after nucleation, the hydrates grow at a faster rate than that with L-valine or L-leucine. Also, it can be clearly observed that there are multiple growth stages in the 0.25 wt% L-methionine solution. However, the length of each growth stage is so short that it could almost be considered as a single stage. With 0.50 wt% L-methionine solution, the hydrates grow almost in a single stage. Moreover, the rate of hydrate formation significantly increases as the L-methionine concentration increases. Surprisingly, at 1.00 wt% L-methionine solution, the methane hydrate growth occurs in a single stage with the highest rate of hydrate formation, and the time taken for 90% completion of hydrate formation (t_{90}) similarly decreases to 34.78 (± 3.35) minutes. The results are consistent with by Cai *et al.* (2017), who reported that the t_{90} was decreased as the L-methionine concentration increased in the CO₂ hydrate formation. As a result, it can be implied that L-methionine effectively promotes methane hydrate formation.

Moreover, the morphology observations during methane hydrate formation using different L-methionine concentrations at 8 MPa and 277.2 K are presented in Figure 4.12. It can be clearly seen that the morphology during the formation in all L-

methionine concentrations shows a similar growth pattern. The hydrates first occur at the vortex interface and concurrently grow upward into the gas phase and downward into the bulk solution, similar to the case of the L-valine system. With 0.25 wt% L-methionine during the hydrate growth, it can also be clearly observed that the hydrates grow downward into the bulk solution with 'bubble-like' formation. As the L-methionine concentration increases, the hydrates grow faster until they completely fill the window within approximately 30 minutes with no further significant morphological changes. Moreover, the characteristics during methane hydrate formation can be clearly seen in Figure 4.13. It can be seen that hydrates grow upward along the reactor wall with the capillary channel effect and downward into the bulk solution with methane bubble. However, these characteristics are not clearly observed at all L-methionine concentrations, due to the solution is evidently moving rapidly along the reactor walls, partly due to the reduction in surface tension caused by L-methionine.



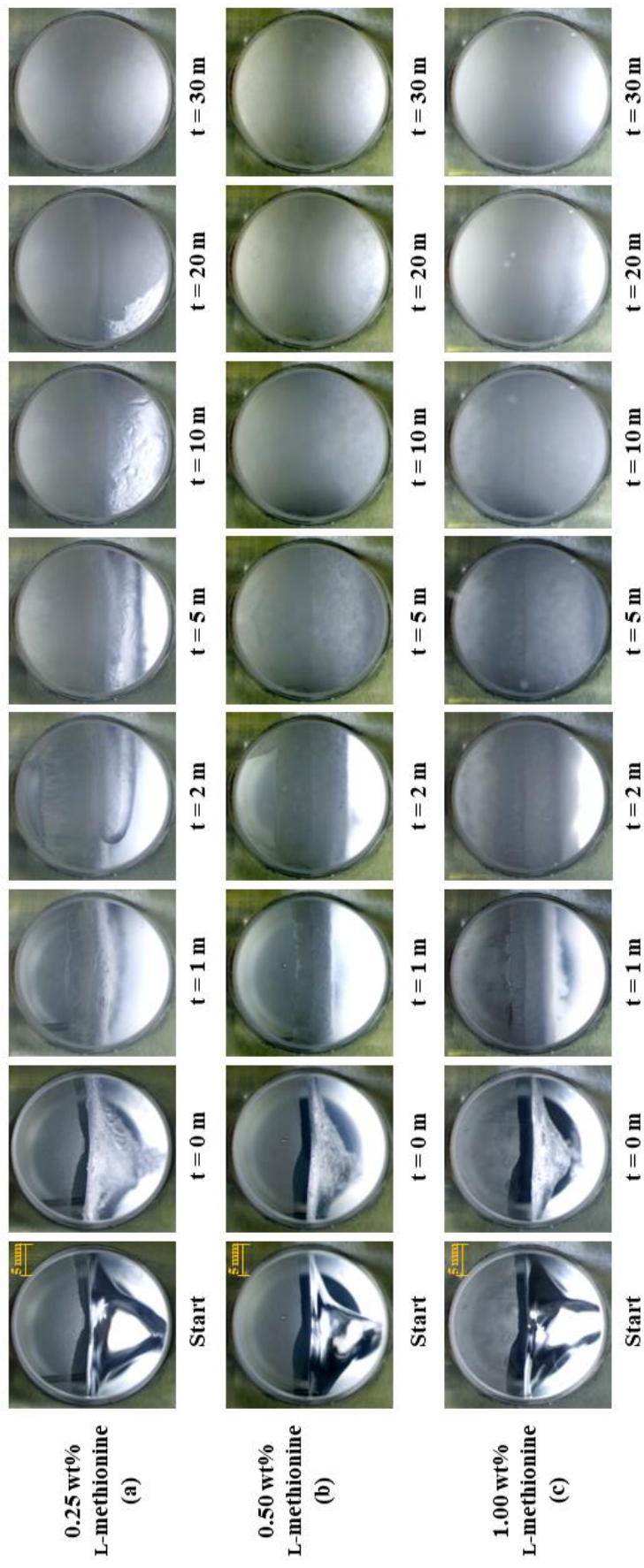


Figure 4.12 Morphology observation during methane hydrate formation using different L-methionine concentrations at 8 MPa and 277.2 K.

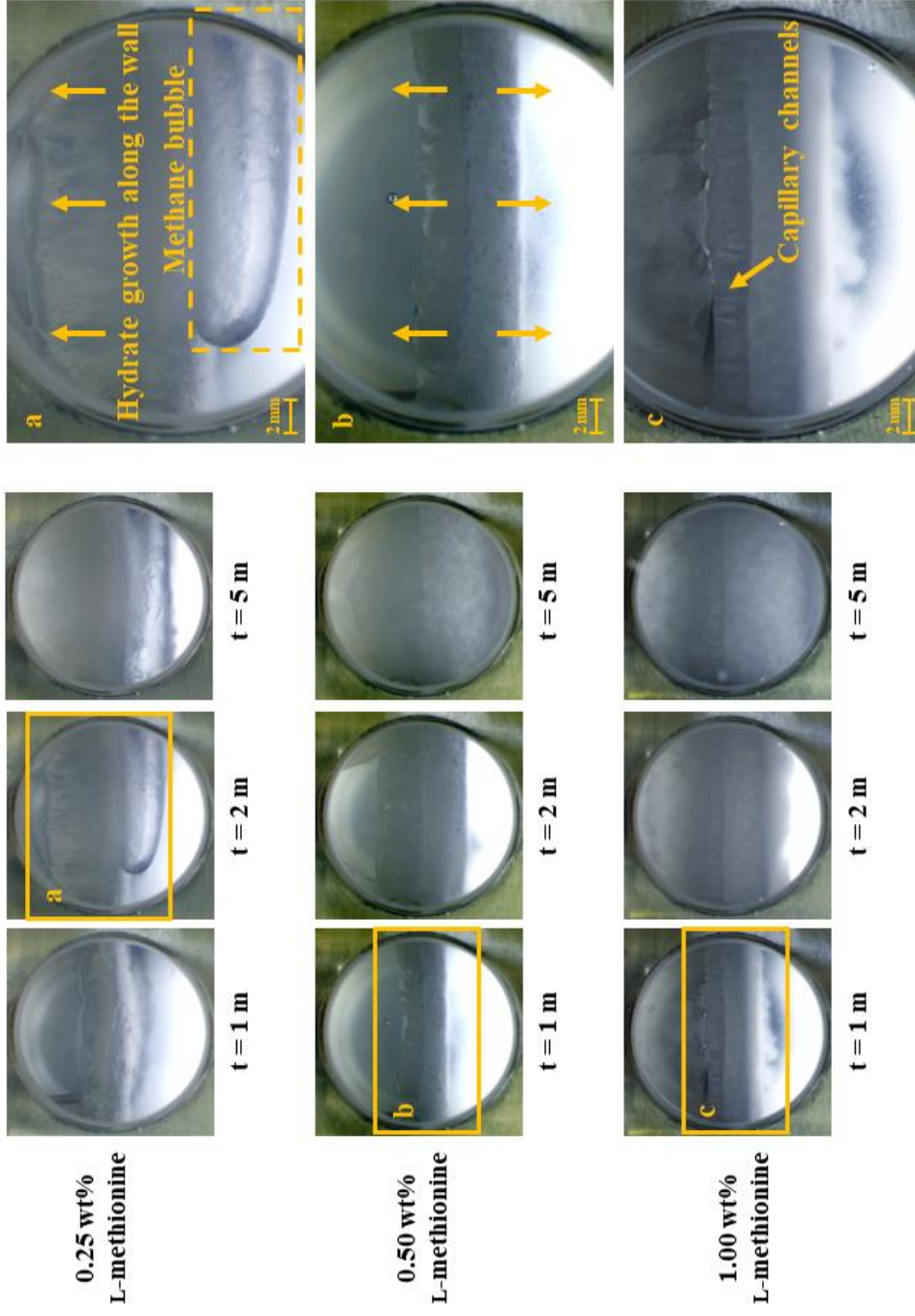


Figure 4.13 Zoomed morphology of methane hydrate formation in the presence of L-methionine.

4.4 Comparative Effect of Amino Acids on Methane Hydrate Formation

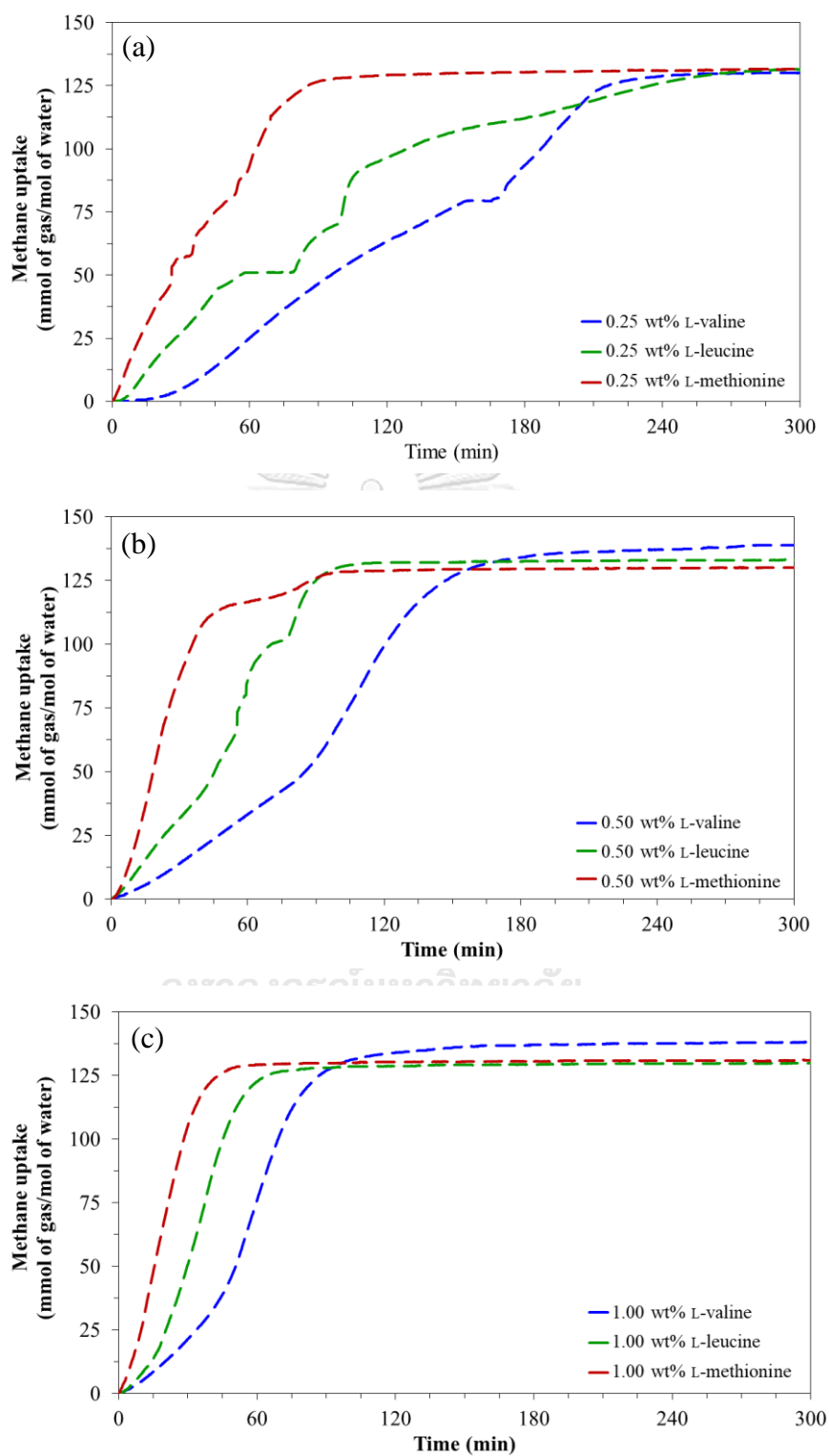


Figure 4.14 Average methane uptake profiles during methane hydrate formation using (a) 0.25 wt%, (b) 0.50 wt%, and (c) 1.00 wt% of different amino acids at 8 MPa and 277.2 K.

Figure 4.14 shows the comparison of the methane uptake profiles during methane hydrate formation with L-valine, L-leucine, and L-methionine. The results show that the amino acids can induce the methane hydrate formation rate and demonstrate a similar final methane uptake. The presence of 1.00 wt% L-methionine promotes methane hydrate formation at the highest rate. Moreover, the induction time with 1.00 wt% L-methionine is the shortest among the amino acids. One interesting aspect of this work is that the final methane uptakes of hydrate formation with L-valine, L-leucine, and L-methionine are nearly comparable to the SDS system under the same conditions (8 MPa and 277.2 K), according to Siangsai *et al.* (2018), they reported that the methane consumed was about 152 mmol of gas/mol of water using 8 mM of SDS. As mentioned earlier, these three amino acids have different aliphatic side chains, which indicates that they have different hydrophobicity. For this reason, it is possible that the hydrophobic property of amino acids affects the methane hydrate formation kinetics. The hydrophathy index is a number that can describe whether an amino acid side chain is hydrophobic or hydrophilic. Generally, the greater the number, the more hydrophobic the amino acid (L-valine has a hydrophathy index of 4.2, which is highly hydrophobic, L-leucine has a hydrophathy index of 3.8, and L-methionine has a low hydrophathy index of 1.9) (Kyte and Doolittle, 1982; Mitaku *et al.*, 2002). The hydrophobic amino acids are exceptionally attractive as kinetic promoters for methane hydrate formation because they are structurally similar to surfactants, which have been widely reported as highly effective kinetic promoters (Bavoh *et al.*, 2019). However, the excessive hydrophobicity of amino acids affects the inhibition of methane hydrate formation. The charge on amino acids enables them to interact strongly with water molecules, disrupting the network of hydrogen bond between water molecules (Sa *et al.*, 2013). L-methionine has the lowest hydrophathy index of all investigated amino acids, but it is still classified as a hydrophobic amino acid. It can effectively promote the methane hydrate formation with the highest rate of hydrate formation by acting as a surfactant that reduces the interfacial surface tension between the gas and liquid phases, allowing gas molecules to permeate easily into the liquid phase and convert to hydrates (Raza *et al.*, 2019; Rodríguez and Romero, 2017). Therefore, L-methionine can be accepted to be an effective kinetic promoter for methane hydrate formation. Moreover, L-methionine effectively enhances hydrate

formation in pure CO₂ and CH₄-CO₂ gas mixture systems (Cai *et al.*, 2017; Prasad and Sai Kiran, 2018; Prasad and Kiran, 2020; Sa *et al.*, 2013). In contrast, highly hydrophobic amino acids (L-leucine and L-valine) have been reported to significantly promote methane hydrate formation (Bavoh *et al.*, 2018; Liu *et al.*, 2015), but exhibit weak or no kinetic promotion in the case of pure CO₂ hydrate formation (Prasad and Sai Kiran, 2018; Prasad and Kiran, 2018; Sa *et al.*, 2013). In addition, the final methane uptake and water to hydrate conversion (shown in Tables 4.1-4.3) present similar results. It can be implied that the presence of amino acids and their concentration only effects on methane hydrate formation kinetics without influencing the thermodynamics. The results of this work are also consistent with the reports by Jeenuang *et al.* (2021) and Inkong *et al.* (2022b).

Although it is obvious that hydrophobic amino acids significantly enhance methane hydrate formation, the mechanism of hydrate formation in the presence of amino acids is not clearly understood. According to a concept proposed by Frank and Evans (1945) and supported by many studies (Bhattacharjee and Linga, 2021; Chandler, 2005; Grdadolnik *et al.*, 2017; Nguyen and Nguyen, 2017), when an amino acid is mixed with water, it forms spontaneously hydrophobic pockets or zones inside the solution. To avoid the hydrophobic amino acid, water molecules strongly aggregate and are generated in the form of a clathrate-like empty cage, known as the hydrophobic hydration shell. In addition, the nonpolar gas molecules (methane) are induced by hydrophobic interactions to assemble around the hydrophobic hydration shells, resulting in an enriched gas density in these zones. The enhanced gas density and the existing hydrophobic hydration shells make the hydrate nucleation occur faster. Therefore, this concept could be used to explain how hydrophobic amino acids promote the methane hydrate formation in this work.

4.5 Hydrate Dissociation

As described in the experimental procedure, the hydrate dissociation experiments were performed using the thermal stimulation method to investigate the decomposition behavior and hydrate stability after completion of methane hydrate formation. The temperature was increased from 277.2 to 298.2 K. The heating rate for

all the conducted experiments was the same. The final methane recovery of all experiments is presented in Tables 4.1-4.3. The final methane recovery in the presence of amino acids at different concentrations is in the range of 95-100%. According to the results, it can be concluded that the presence of amino acids has no effect on the final methane recovery.

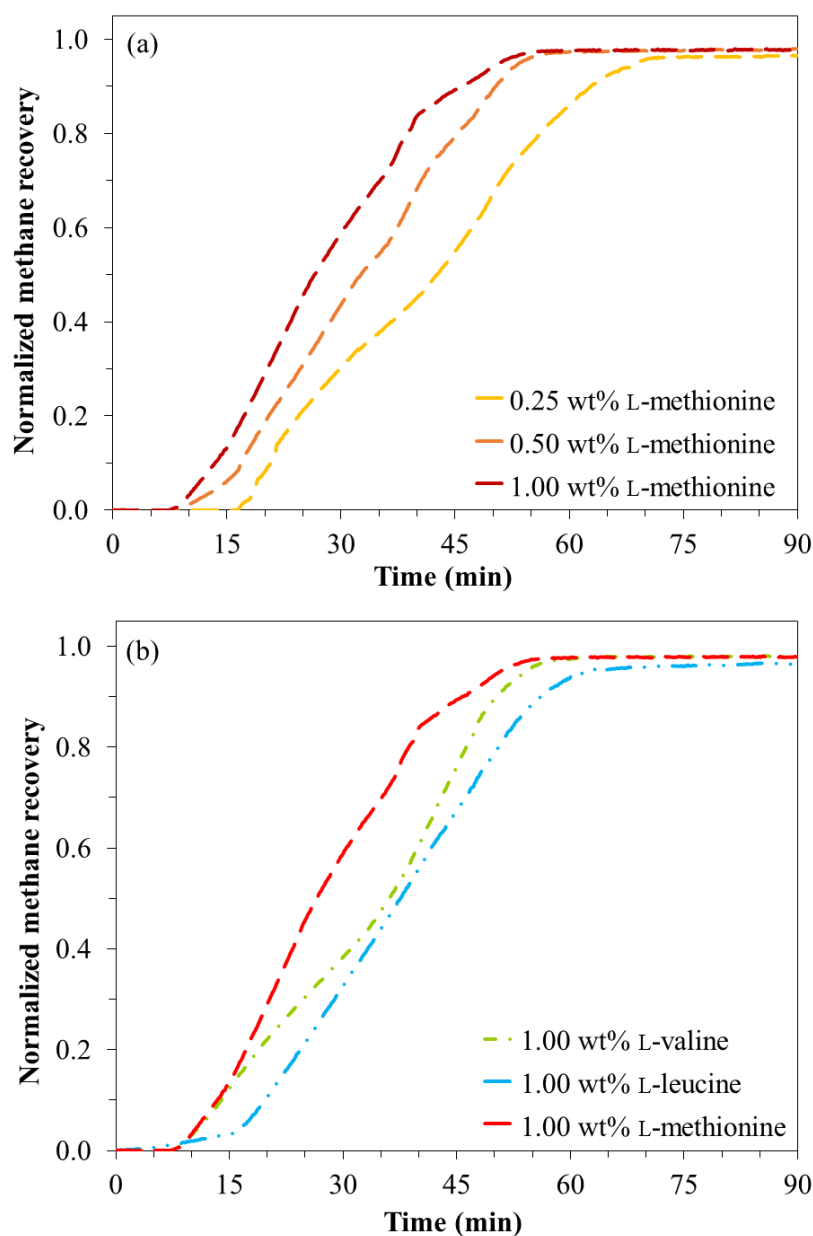
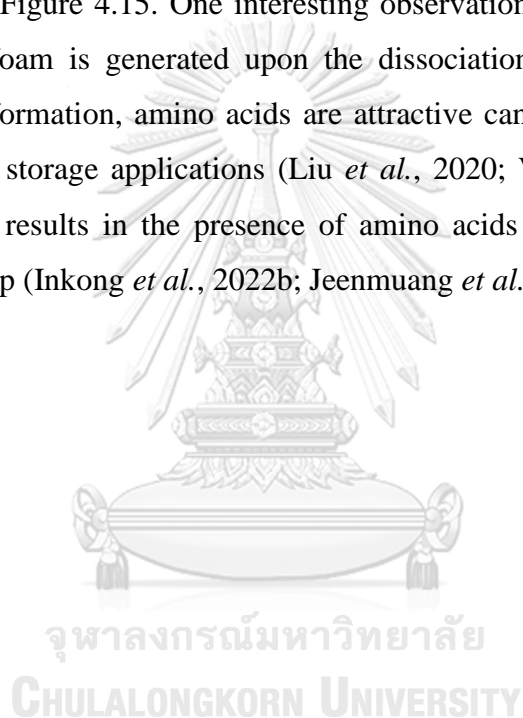


Figure 4.15 Average normalized methane recovery profiles during methane hydrate dissociation in the presence of (a) different amino acid concentration and (b) different amino acids.

To further investigate the effects of amino acids on the hydrate dissociation kinetics, the average normalized methane recovery profiles are presented in Figure 4.15. The effect of different amino acid concentrations on the hydrate dissociation kinetics is represented by the dissociation of hydrates formed with L-methionine at different concentrations, Figure 4.15a. As seen in the figure, the gas released at the beginning of the process (about 0-8 minutes) is not observed because the hydrate dissociation process is an endothermic process that requires heat to dissociate the hydrogen bonds of the formed hydrate cages. It can be observed that the rate of hydrate dissociation increases as the L-methionine concentration increases. This result corresponds with the reports by Ganji *et al.* (2007) and Lin *et al.* (2004) for the dissociation of methane hydrates. The presence of amino acids decreases the formed hydrate particle size, resulting in a vastly larger surface area (Ganji *et al.*, 2007). Heat transfer is faster due to the larger surface area. Therefore, the amino acid concentration results in an increase in the hydrate dissociation rate. Another point is that the effect of different amino acids on the hydrate dissociation kinetics is represented by the dissociation of hydrates formed with different amino acids at 1.00 wt% concentration, Figure 4.15b. Obviously, it can be seen that the time required to decompose the methane hydrates formed with L-methionine and L-valine is shorter than that with L-leucine. As a result, the hydrate formed with L-methionine and L-valine systems need less heat to start the dissociation process. Furthermore, the hydrates formed with L-methionine, L-leucine, and L-valine completely dissociate within 55, 58, and 70 minutes in, respectively.

Additionally, Figure 4.16 presents the morphology observations during the hydrate dissociation in the presence of amino acids. It can be observed that the hydrate dissociation patterns are similar in all systems. However, differences in time between each phase of dissociation can be observed. After about 40 minutes from the beginning of hydrate dissociation, it can be seen that the traces of hydrates start to decompose along the sapphire window. Since the reactor is surrounded by heated water, the heat is transferred directly to the reactor wall. As seen in the sapphire window around 5-10 minutes later, the progressive decomposition of the hydrate layer occurs along the window. Following that, the hydrate clusters decompose constantly, revealing the regenerated solution at the bottom of the reactor (about 50-60 minutes

after the start of hydrate dissociation). Within 70 minutes following the initiation of hydrate dissociation, the hydrate clusters are completely decomposed, as only the solution is present in the reactor. However, the decomposition of hydrates formed using 0.25 wt% L-methionine is quite slower than that using 1.00 wt% L-methionine, as shown in Figures 4.16a and 4.16b. When comparing each amino acid at the same concentration (1.00 wt%), the L-valine and L-methionine systems decompose faster than the L-leucine system, as can be clearly seen in Figures 4.16b-4.16d. These morphological observations are consistent with the normalized methane recovery profiles shown in Figure 4.15. One interesting observation in the presence of amino acids is that no foam is generated upon the dissociation of hydrates. Due to the absence of foam formation, amino acids are attractive candidates for deployment in hydrate-based gas storage applications (Liu *et al.*, 2020; Veluswamy *et al.*, 2016a). Moreover, all the results in the presence of amino acids correspond with previous studies in our group (Inkong *et al.*, 2022b; Jeenuang *et al.*, 2021).



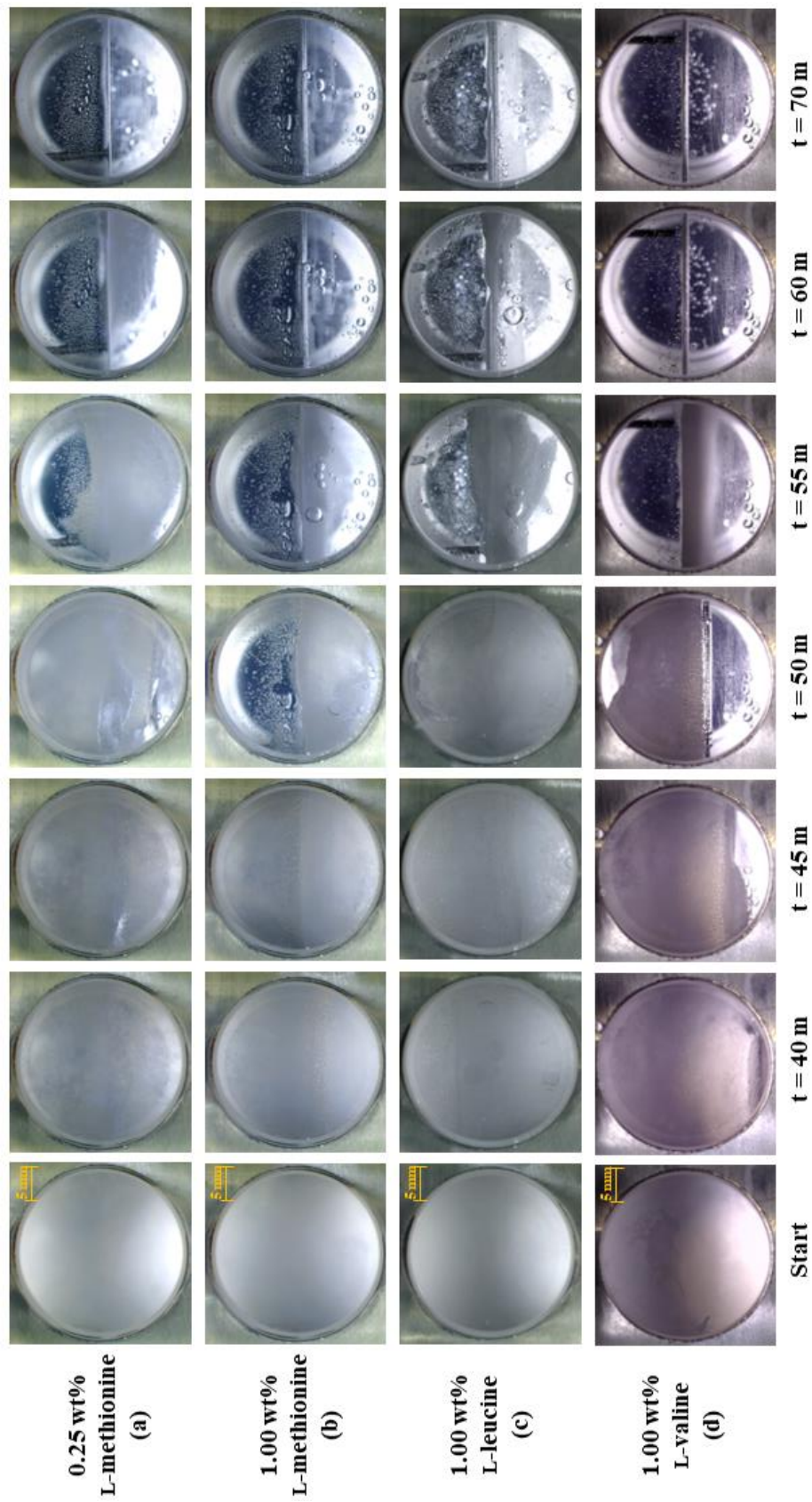


Figure 4.16 Morphology observations during methane hydrate dissociation using different amino acids with different concentrations at 8 MPa and 277.2 K.

Subsequently, the effects of memory solution on the methane hydrate formation at 8 MPa and 277.2 K were investigated by repeating the experiments with the reused solution. After completion of hydrate dissociation, the used methane gas is gradually released from the reactor. Then, the system is reset with the original experiment conditions. All kinetic results in both fresh and reused solutions are summarized in Table 4.4. As can be observed, the induction time is reduced in the memory experiments. This is because some amount of methane gas remains dissolved in the solution due to incomplete methane recovery. When the stirring is started, the existence of dissolved methane in the reused solution could induce the hydrate nucleation to occur faster than in the fresh solution (Makogon, 1997; Wu and Zhang, 2010). However, it can be observed that there is no significant difference in the NR_{30} and the t_{90} between fresh and reused solution systems. Furthermore, the final methane uptakes achieved from the fresh and reused solutions of amino acids are presented in Figure 4.17. There is no significant difference in the final methane uptake between fresh and reused solution systems. It can be implied that the methane hydrate formation in the presence of amino acids can occur again with similar efficiency. Therefore, it can be confirmed that amino acids are the effective kinetic promoters in methane hydrate formation for SNG technology and gas storage applications.

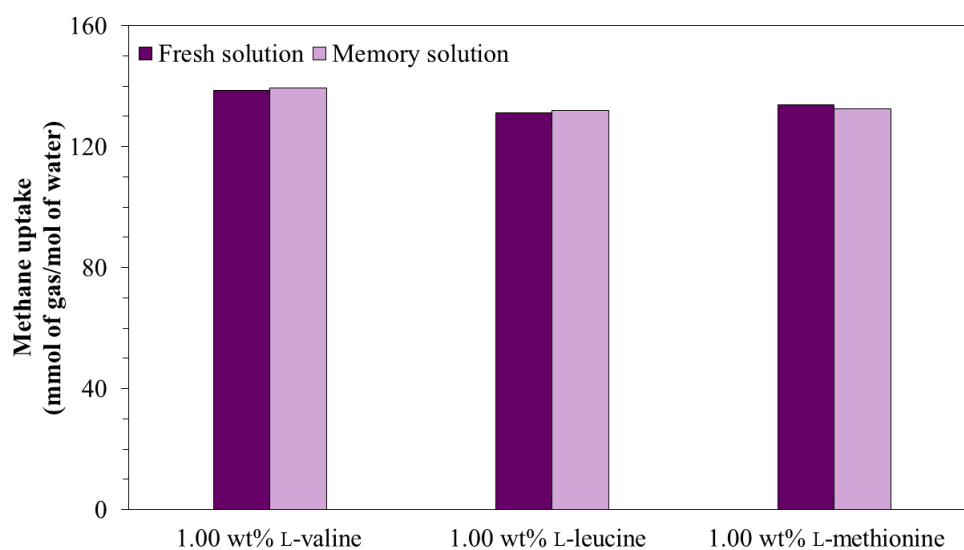


Figure 4.17 Final methane uptakes achieved from the fresh and reused solutions of 1.00 wt% L-valine, L-leucine, and L-methionine at 8 Mpa and 277.2 K.

Table 4.4 Experimental results for methane hydrate formation using fresh and reused solutions 8 MPa and 277.2 K

Amino acid conc. (wt%)	No. Exp.	^a Induction time (min)	^b NR ₃₀ (kmol of gas/ m ³ of water/hr)	^c t ₉₀ (min)	Methane uptake (mmol of gas/ mol of water)	Water to hydrate conversion (%)	% Methane recovery
L-valine							
0.25	A1	56.47	0.44	198.83	122.91	70.68	97.30
	AM1	49.33	0.50	159.83	133.82	76.95	96.34
0.50	B1	49.07	1.48	138.17	133.15	76.56	97.24
	BM1	29.47	1.61	115.83	134.22	77.17	97.83
1.00	C1	26.53	2.64	95.50	138.70	79.75	96.47
	CM1	25.63	2.11	87.50	139.32	80.11	98.11
L-leucine							
0.25	D1	24.17	3.28	249.33	132.49	76.18	97.48
	DM1	16.40	3.77	133.83	126.86	72.95	97.99
0.50	E1	22.73	3.76	67.33	136.29	78.37	97.84
	EM1	22.23	3.67	69.00	135.68	78.02	97.17
1.00	F1	16.63	5.38	55.83	131.30	73.14	95.89
	FM1	10.33	5.70	54.50	132.04	73.54	96.10

Table 4.4 (Continued) Experimental results for methane hydrate formation using fresh and reused solutions 8 MPa and 277.2 K

Amino acid conc. (wt%)	No. Exp.	^a Induction time (min)	^b NR ₃₀ (kmol of gas/ m ³ of water/hr)	^c t ₉₀ (min)	Methane uptake (mmol of gas/ mol of water)	Water to hydrate conversion (%)	% Methane recovery
L-methionine							
0.25	G1	19.57	6.68	48.50	132.84	76.38	97.71
	GM1	17.53	6.49	69.33	131.34	75.52	96.97
0.50	H1	22.30	10.11	41.33	134.57	77.38	98.42
	HM1	22.63	10.05	41.00	135.06	77.66	98.47
1.00	I1	20.23	12.05	38.67	133.77	76.92	98.93
	IM1	19.60	12.07	42.50	132.60	76.25	97.50

^a Induction time is the time interval between the starting point of the experiment (the stirring started) and the nucleation of the first hydrate crystal (the stirring stopped).

^b NR₃₀ is the normalized rate of hydrate formation 30 minutes from the induction time.

^c t₉₀ is the time required to reach 90% of the final methane uptake calculated from the nucleation.

CHAPTER 5

CONCLUSION AND RECOMMENDATIONS

5.1 Conclusion

In this work, the methane hydrate formation using three different amino acids was investigated at 8 MPa and 277.2 K using the HCR approach. By increasing the surface contact area, the HCR approach effectively overcomes the limitation of gas transfer into the liquid phase, thus improving hydrate nucleation and reducing the induction time. Three amino acids significantly enhance the hydrate formation rate and decrease the induction time, especially in L-methionine. With low amino acid concentrations, the deflection points are observed during the methane hydrate formation due to the lower amount of amino acid, resulting in ineffectively promoting the methane hydrate formation. Moreover, these effects become more apparent as the amino acid concentration increases. However, these three amino acids show similar results with no effect on the final methane uptake and the water to hydrate conversion. The morphology observation during the hydrate formation in the presence of each amino acid shows that the hydrate nucleation occurs at the gas-liquid interface. Then, hydrates grow upward along the reactor wall and downward into the bulk solution. Finally, the hydrates grow densely until they cover the entire window. Methane recovery is greater than 95%, and there is no foam formation during the dissociation process in all experiments. Moreover, three amino acids in the reused solutions can promote the second formation with the same results as the first formation.

5.2 Recommendations

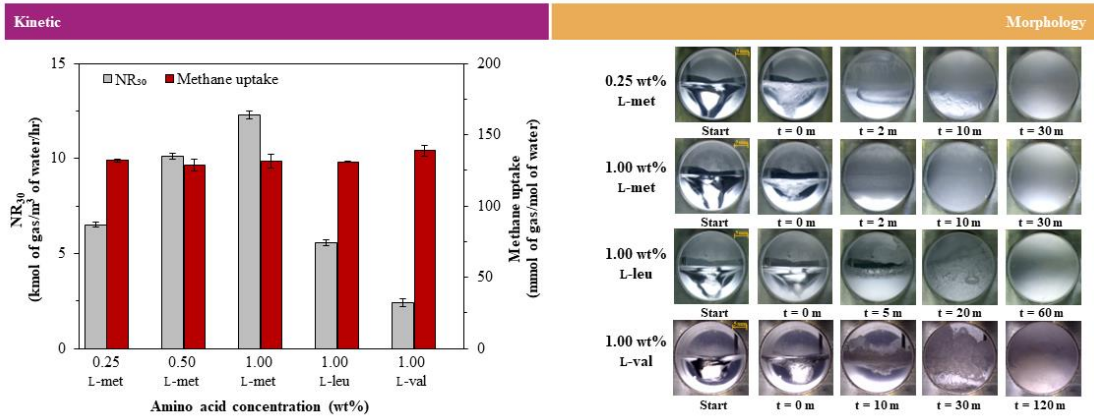
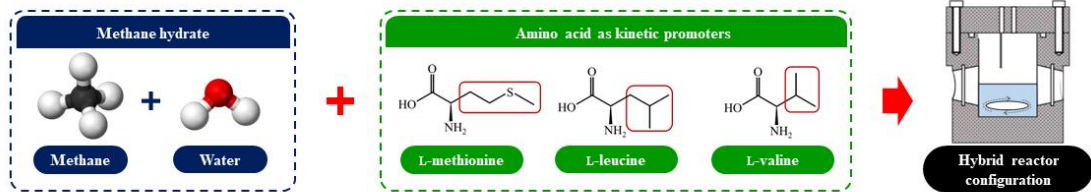
To obtain more understanding of the effect of amino acids on methane hydrate formation, studies using other amino acids should be performed. In addition, an in-depth study of the memory effect should also be carried out, including an analysis of the amino acid content remaining after each hydrate formation. For the variety of gas hydrate applications, this investigated system should be applied to study the CO₂ hydrate and mixed gas hydrate formation.

APPENDIX

GRAPHICAL ABSTRACT

Appendix A

Methane hydrate formation in the presence of biofriendly amino acids



REFERENCES

- Babu, P., Kumar, R., and Linga, P. (2013). Pre-combustion capture of carbon dioxide in a fixed bed reactor using the clathrate hydrate process. Energy, 50, 364-373.
- Babu, P., Nambiar, A., He, T., Karimi, I. A., Lee, J. D., Englezos, P., and Linga, P. (2018). A review of clathrate hydrate based desalination to strengthen energy–water nexus. ACS Sustainable Chemistry & Engineering, 6(7), 8093-8107.
- Bavoh, C. B., Lal, B., Osei, H., Sabil, K. M., and Mukhtar, H. (2019). A review on the role of amino acids in gas hydrate inhibition, CO₂ capture and sequestration, and natural gas storage. Journal of Natural Gas Science and Engineering, 64, 52-71.
- Bavoh, C. B., Nashed, O., Khan, M. S., Partoon, B., Lal, B., and Sharif, A. M. (2018). The impact of amino acids on methane hydrate phase boundary and formation kinetics. The Journal of Chemical Thermodynamics, 117, 48-53.
- Belton, J., and Twidle, A. (1940). The surface tensions of amino-acid solutions as a function of p H. Transactions of the Faraday Society, 36, 1198-1208.
- Bhattacharjee, G., Goh, M. N., Arumuganainar, S. E., Zhang, Y., and Linga, P. (2020). Ultra-rapid uptake and the highly stable storage of methane as combustible ice. Energy & Environmental Science, 13(12), 4946-4961.
- Bhattacharjee, G., and Linga, P. (2021). Amino acids as kinetic promoters for gas hydrate applications: a mini review. Energy & Fuels, 35(9), 7553-7571.
- Botimer, J. D., Dunn-Rankin, D., and Taborek, P. (2016). Evidence for immobile transitional state of water in methane clathrate hydrates grown from surfactant solutions. Chemical Engineering Science, 142, 89-96.
- Buffett, B. A. (2000). Clathrate hydrates. Annual Review of Earth and Planetary Sciences, 28(1), 477-507.
- Cai, Y., Chen, Y., Li, Q., Li, L., Huang, H., Wang, S., and Wang, W. (2017). CO₂ hydrate formation promoted by a natural amino acid l-methionine for possible application to CO₂ capture and storage. Energy Technology, 5(8), 1195-1199.
- Carroll, J. (2020). Natural gas hydrates: a guide for engineers: Gulf Professional Publishing.
- Chandler, D. (2005). Interfaces and the driving force of hydrophobic assembly. Nature, 437(7059), 640-647.

- Christuansen, R. L., and Sloan, J. E. D. (1994). Mechanisms and kinetics of hydrate formation. Annals of the New York Academy of Sciences, 715(1), 283-305.
- Costandy, J., Michalis, V. K., Stubos, A. K., Tsimpanogiannis, I. N., and Economou, I. G. (2015). Atomistic simulations of clathrate hydrates. In M. J. Al-Marri and F. T. Eljack (Eds.), Proceedings of the 4th International Gas Processing Symposium (pp. 351-359). Oxford: Elsevier.
- Du, J., Li, H., and Wang, L. (2014). Effects of ionic surfactants on methane hydrate formation kinetics in a static system. Advanced Powder Technology, 25(4), 1227-1233.
- EIA. (2020). Gas 2020. Retrieved from <https://www.iea.org/reports/gas-2020>
- EIA. (2021). Global energy review 2021: assessing the effects of economic recoveries on global energy demand and CO2 emissions in 2021. Retrieved from <https://iea.blob.core.windows.net/assets/d0031107-401d-4a2f-a48b-9eed19457335/GlobalEnergyReview2021.pdf>
- Eslamimanesh, A., Mohammadi, A. H., Richon, D., Naidoo, P., and Ramjugernath, D. (2012). Application of gas hydrate formation in separation processes: A review of experimental studies. The Journal of Chemical Thermodynamics, 46, 62-71.
- Frank, H. S., and Evans, M. W. (1945). Free volume and entropy in condensed systems III. entropy in binary liquid mixtures; partial molal entropy in dilute solutions; structure and thermodynamics in aqueous electrolytes. The Journal of Chemical Physics, 13(11), 507-532.
- Ganji, H., Manteghian, M., Sadaghiani zadeh, K., Omidkhah, M. R., and Rahimi Mofrad, H. (2007). Effect of different surfactants on methane hydrate formation rate, stability and storage capacity. Fuel, 86(3), 434-441.
- Gliński, J., Chavepeyer, G., and Platten, J. (2000). Surface properties of aqueous solutions of L-leucine. Biophysical chemistry, 84, 99-103.
- Grdadolnik, J., Merzel, F., and Avbelj, F. (2017). Origin of hydrophobicity and enhanced water hydrogen bond strength near purely hydrophobic solutes. Proceedings of the National Academy of Sciences, 114(2), 322-327.
- Hammerschmidt, E. G. (1934). Formation of gas hydrates in natural gas transmission lines. Industrial & Engineering Chemistry, 26(8), 851-855.

- Inkong, K., Anh, L. T., Yodpetch, V., Kulprathipanja, S., and Rangsunvigit, P. (2022a). An insight on effects of activated carbon and a co-promoter on carbon dioxide hydrate formation and dissociation. Chemical Engineering Science, 248, 117100.
- Inkong, K., Rangsunvigit, P., Kulprathipanja, S., and Linga, P. (2019a). Effects of temperature and pressure on the methane hydrate formation with the presence of tetrahydrofuran (THF) as a promoter in an unstirred tank reactor. Fuel, 255, 115705.
- Inkong, K., Veluswamy, H. P., Rangsunvigit, P., Kulprathipanja, S., and Linga, P. (2019b). Innovative approach to enhance the methane hydrate formation at near-ambient temperature and moderate pressure for gas storage applications. Industrial & Engineering Chemistry Research, 58(49), 22178-22192.
- Inkong, K., Veluswamy, H. P., Rangsunvigit, P., Kulprathipanja, S., and Linga, P. (2019c). Investigation on the kinetics of methane hydrate formation in the presence of methyl ester sulfonate. Journal of Natural Gas Science and Engineering, 71, 102999.
- Inkong, K., Yodpetch, V., Kulprathipanja, S., Rangsunvigit, P., and Linga, P. (2022b). Influences of different co-promoters on the mixed methane hydrate formation with salt water at moderate conditions. Fuel, 316, 123215.
- Jeenmuang, K., Viriyakul, C., Inkong, K., Prakash Veluswamy, H., Kulprathipanja, S., Rangsunvigit, P., and Linga, P. (2021). Enhanced hydrate formation by natural-like hydrophobic side chain amino acids at ambient temperature: A kinetics and morphology investigation. Fuel, 299, 120828.
- Kalogerakis, N., Jamaluddin, A. K. M., Dholabhai, P. D., and Bishnoi, P. R. (1993). Effect of surfactants on hydrate formation kinetics. Paper presented at the SPE International Symposium on Oilfield Chemistry.
- Khurana, M., Yin, Z., and Linga, P. (2017). A review of clathrate hydrate nucleation. ACS Sustainable Chemistry & Engineering, 5(12), 11176-11203.
- Kondori, J., Zendeheboudi, S., and Hossain, M. E. (2017). A review on simulation of methane production from gas hydrate reservoirs: Molecular dynamics prospective. Journal of Petroleum Science and Engineering, 159, 754-772.
- Kumar, A., Bhattacharjee, G., Kulkarni, B. D., and Kumar, R. (2015). Role of

- surfactants in promoting gas hydrate formation. Industrial & Engineering Chemistry Research, 54(49), 12217-12232.
- Kyte, J., and Doolittle, R. F. (1982). A simple method for displaying the hydrophobic character of a protein. Journal of Molecular Biology, 157(1), 105-132.
- Lederhos, J., Mehta, A., Nyberg, G., Warn, K., and Sloan, E. (1992). Structure H clathrate hydrate equilibria of methane and adamantane. AIChE journal, 38(7), 1045-1048.
- Lederhos, J. P., Long, J. P., Sum, A., Christiansen, R. L., and Sloan, E. D. (1996). Effective kinetic inhibitors for natural gas hydrates. Chemical Engineering Science, 51(8), 1221-1229.
- Lin, W., Chen, G. J., Sun, C. Y., Guo, X. Q., Wu, Z. K., Liang, M. Y., Chen, L. T., and Yang, L. Y. (2004). Effect of surfactant on the formation and dissociation kinetic behavior of methane hydrate. Chemical Engineering Science, 59(21), 4449-4455.
- Linga, P., Daraboina, N., Ripmeester, J. A., and Englezos, P. (2012). Enhanced rate of gas hydrate formation in a fixed bed column filled with sand compared to a stirred vessel. Chemical Engineering Science, 68(1), 617-623.
- Linga, P., Haligva, C., Nam, S. C., Ripmeester, J. A., and Englezos, P. (2009). Recovery of methane from hydrate formed in a variable volume bed of silica sand particles. Energy & Fuels, 23(11), 5508-5516.
- Linga, P., Kumar, R., Lee, J. D., Ripmeester, J., and Englezos, P. (2010). A new apparatus to enhance the rate of gas hydrate formation: Application to capture of carbon dioxide. International Journal of Greenhouse Gas Control, 4(4), 630-637.
- Liu, Y., Chen, B., Chen, Y., Zhang, S., Guo, W., Cai, Y., Tan, B., and Wang, W. (2015). Methane storage in a hydrated form as promoted by leucines for possible application to natural gas transportation and storage. Energy Technology, 3(8), 815-819.
- Liu, Z., Zeng, Y., and Wang, W. (2020). CO₂ hydrate formation promoted by a bio-friendly amino acid L - Isoleucine. Paper presented at the IOP Conference Series: Earth and Environmental Science.
- Makogon, I. U. r. F. (1981). Hydrates of natural gas: PennWell Books Tulsa, Oklahoma.

- Makogon, Y. F. (1997). Hydrates of hydrocarbons.
- Mao, W. L., Mao, H.-k., Goncharov, A. F., Struzhkin, V. V., Guo, Q., Hu, J., Shu, J., Hemley, R. J., Somayazulu, M., and Zhao, Y. (2002). Hydrogen clusters in clathrate hydrate. Science, 297(5590), 2247.
- Mitaku, S., Hirokawa, T., and Tsuji, T. (2002). Amphiphilicity index of polar amino acids as an aid in the characterization of amino acid preference at membrane–water interfaces. Bioinformatics, 18(4), 608-616.
- Mokhatab, S., and Poe, W. A. (2012). Handbook of natural gas transmission and processing: Gulf professional publishing.
- Morlat, M., Pernolet, R., and Gerard, N. (1976). Formation process of ethylene hydrate. Paper presented at the Proceeding of International Symposium on Fresh Water from Sea, Alghero, Italy.
- Naeiji, P., Arjomandi, A., and Varaminian, F. (2014). Amino acids as kinetic inhibitors for tetrahydrofuran hydrate formation: Experimental study and kinetic modeling. Journal of Natural Gas Science and Engineering, 21, 64-70.
- Nakamura, T., Makino, T., Sugahara, T., and Ohgaki, K. (2003). Stability boundaries of gas hydrates helped by methane—structure-H hydrates of methylcyclohexane and cis-1, 2-dimethylcyclohexane. Chemical Engineering Science, 58(2), 269-273.
- Nguyen, N. N., and Nguyen, A. V. (2017). Hydrophobic effect on gas hydrate formation in the presence of additives. Energy & Fuels, 31(10), 10311-10323.
- Ohmura, R., Matsuda, S., Uchida, T., Ebinuma, T., and Narita, H. (2005). Clathrate hydrate crystal growth in liquid water saturated with a guest substance: observations in a methane + water system. Crystal Growth & Design, 5(3), 953-957.
- Pandey, G., Bhattacharjee, G., Veluswamy, H. P., Kumar, R., Sangwai, J. S., and Linga, P. (2018). Alleviation of foam formation in a surfactant driven gas hydrate system: insights via a detailed morphological study. ACS Applied Energy Materials, 1(12), 6899-6911.
- Pandey, J. S., Daas, Y. J., and von Solms, N. (2020a). Methane hydrate formation, storage and dissociation behavior in unconsolidated sediments in the presence of

- environment-friendly promoters. Paper presented at the SPE Europec.
- Pandey, J. S., Jouljamal Daas, Y., Paul Karcz, A., and Solms, N. v. (2020b). Methane hydrate formation behavior in the presence of selected amino acids. Journal of Physics: Conference Series, 1580, 012003.
- Partoon, B., Malik, S. N. A., Azemi, M. H., and Sabil, K. M. (2013). Experimental investigations on the potential of SDS as low-dosage promoter for carbon dioxide hydrate formation. Asia-Pacific Journal of Chemical Engineering, 8(6), 916-921.
- Prasad, P. S., and Sai Kiran, B. (2018). Clathrate hydrates of greenhouse gases in the presence of natural amino acids: storage, transportation and separation applications. Scientific reports, 8(1), 1-10.
- Prasad, P. S. R., and Kiran, B. S. (2018). Are the amino acids thermodynamic inhibitors or kinetic promoters for carbon dioxide hydrates? Journal of Natural Gas Science and Engineering, 52, 461-466.
- Prasad, P. S. R., and Kiran, B. S. (2020). Synergistic effects of amino acids in clathrate hydrates: Gas capture and storage applications. Chemical Engineering Journal Advances, 3, 100022.
- Raza, M. A., Hallett, P. D., Liu, X., He, M., and Afzal, W. (2019). Surface tension of aqueous solutions of small-chain amino and organic acids. Journal of Chemical & Engineering Data, 64(12), 5049-5056.
- Rodríguez, D. M., and Romero, C. M. (2017). Surface tension of glycine, alanine, aminobutyric acid, norvaline, and norleucine in water and in aqueous solutions of strong electrolytes at temperatures from (293.15 to 313.15 K). Journal of Chemical & Engineering Data, 62(11), 3687-3696.
- Sa, J.-H., Kwak, G.-H., Lee, B. R., Park, D.-H., Han, K., and Lee, K.-H. (2013). Hydrophobic amino acids as a new class of kinetic inhibitors for gas hydrate formation. Scientific reports, 3(1), 2428.
- Sharma, S., Saxena, A., and Saxena, N. (2019). Application of gas hydrates. In *Unconventional Resources in India: The Way Ahead* (pp. 69-73). Cham: Springer International Publishing.
- Shin, W., Park, S., Koh, D.-Y., Seol, J., Ro, H., and Lee, H. (2011). Water-soluble

- structure H clathrate hydrate formers. The Journal of Physical Chemistry C, 115(38), 18885-18889.
- Siangsai, A., Inkong, K., Kulprathipanja, S., Kitiyanan, B., and Rangsunvigit, P. (2018). Roles of sodium dodecyl sulfate on tetrahydrofuran-assisted methane hydrate formation. Journal of Oleo Science, 67.
- Siangsai, A., Rangsunvigit, P., Kitiyanan, B., Kulprathipanja, S., and Linga, P. (2015). Investigation on the roles of activated carbon particle sizes on methane hydrate formation and dissociation. Chemical Engineering Science, 126, 383-389.
- Siažik, J., Malcho, M., and Lenhard, R. (2017). Proposal of experimental device for the continuous accumulation of primary energy in natural gas hydrates. EPJ Web of Conferences, 143, 02106.
- Sloan, E. D. (2003). Fundamental principles and applications of natural gas hydrates. Nature, 426(6964), 353-359.
- Sloan Jr, E. D., and Koh, C. A. (2007). Clathrate hydrates of natural gases: CRC press.
- Strobel, T. A., Hester, K. C., Koh, C. A., Sum, A. K., and Sloan, E. D. (2009). Properties of the clathrates of hydrogen and developments in their applicability for hydrogen storage. Chemical Physics Letters, 478(4), 97-109.
- Sun, Q., and Kang, Y. (2016). Review on CO₂ hydrate formation/dissociation and its cold energy application. Renewable and Sustainable Energy Reviews, 62, 478-494.
- Sun, X., Liu, D., Chang, D., Wang, W., and Pan, Z. (2018). Analysis of natural gas hydrate formation in sodium dodecyl sulfate and quartz sand complex system under saline environment. Petroleum Science and Technology, 36(14), 1073-1079.
- Thomas, S., and Dawe, R. A. (2003). Review of ways to transport natural gas energy from countries which do not need the gas for domestic use. Energy, 28(14), 1461-1477.
- Uchida, T., Ebinuma, T., Kawabata, J. i., and Narita, H. (1999). Microscopic observations of formation processes of clathrate-hydrate films at an interface between water and carbon dioxide. Journal of Crystal Growth, 204(3), 348-356.
- Veluswamy, H., Chen, J., and Linga, P. (2015). Surfactant effect on the kinetics of

- mixed hydrogen/propane hydrate formation for hydrogen storage as clathrates. Chemical Engineering Science, 126, 488-499.
- Veluswamy, H. P., Hong, Q. W., and Linga, P. (2016a). Morphology study of methane hydrate formation and dissociation in the presence of amino acid. Crystal Growth & Design, 16(10), 5932-5945.
- Veluswamy, H. P., Kumar, A., Kumar, R., and Linga, P. (2017a). An innovative approach to enhance methane hydrate formation kinetics with leucine for energy storage application. Applied Energy, 188, 190-199.
- Veluswamy, H. P., Kumar, A., Seo, Y., Lee, J. D., and Linga, P. (2018). A review of solidified natural gas (SNG) technology for gas storage via clathrate hydrates. Applied Energy, 216, 262-285.
- Veluswamy, H. P., Kumar, S., Kumar, R., Rangsunvigit, P., and Linga, P. (2016b). Enhanced clathrate hydrate formation kinetics at near ambient temperatures and moderate pressures: Application to natural gas storage. Fuel, 182, 907-919.
- Veluswamy, H. P., Lee, P. Y., Premasinghe, K., and Linga, P. (2017b). Effect of biofriendly amino acids on the kinetics of methane hydrate formation and dissociation. Industrial & Engineering Chemistry Research, 56(21), 6145-6154.
- Veluswamy, H. P., Wong, A. J. H., Babu, P., Kumar, R., Kulprathipanja, S., Rangsunvigit, P., and Linga, P. (2016c). Rapid methane hydrate formation to develop a cost effective large scale energy storage system. Chemical Engineering Journal, 290, 161-173.
- Viriyakul, C., Jeenuang, K., Inkong, K., Kulprathipanja, S., and Rangsunvigit, P. (2021). A detailed morphology investigation on the effects of mixed anionic and nonionic surfactants on methane hydrate formation and dissociation. Journal of Natural Gas Science and Engineering, 90, 103904.
- Wang, F., Jia, Z.-Z., Luo, S.-J., Fu, S.-F., Wang, L., Shi, X.-S., Wang, C.-S., and Guo, R.-B. (2015). Effects of different anionic surfactants on methane hydrate formation. Chemical Engineering Science, 137, 896-903.
- Wu, Q., and Zhang, B. (2010). Memory effect on the pressure-temperature condition and induction time of gas hydrate nucleation. Journal of Natural Gas Chemistry, 19(4), 446-451.

- Yang, M., Zhao, J., Zheng, J.-n., and Song, Y. (2019). Hydrate reformation characteristics in natural gas hydrate dissociation process: A review. Applied Energy, 256, 113878.
- Yoslim, J., Linga, P., and Englezos, P. (2010). Enhanced growth of methane–propane clathrate hydrate crystals with sodium dodecyl sulfate, sodium tetradecyl sulfate, and sodium hexadecyl sulfate surfactants. Journal of Crystal Growth, 313(1), 68-80.
- You, K., Flemings, P. B., Malinverno, A., Collett, T. S., and Darnell, K. (2019). Mechanisms of methane hydrate formation in geological systems. Reviews of Geophysics, 57(4), 1146-1196.
- Zhang, J. S., Lee, S., and Lee, J. W. (2007). Kinetics of methane hydrate formation from SDS solution. Industrial & Engineering Chemistry Research, 46(19), 6353-6359.
- Zhang, P., Wu, Q., and Mu, C. (2017). Influence of temperature on methane hydrate formation. Scientific reports, 7(1), 1-13.
- Zhong, D.-L., Lu, Y.-Y., Sun, D.-J., Zhao, W.-L., and Li, Z. (2015). Performance evaluation of methane separation from coal mine gas by gas hydrate formation in a stirred reactor and in a fixed bed of silica sand. Fuel, 143, 586-594.





จุฬาลงกรณ์มหาวิทยาลัย
CHULALONGKORN UNIVERSITY

VITA

NAME Chuvich Chaovarin

DATE OF BIRTH 8 February 1998

PLACE OF BIRTH Bangkok

INSTITUTIONS ATTENDED 2020-2021 Master of Science in Petrochemical Technology, The Petroleum and Petrochemical College, Chulalongkorn University, Bangkok, Thailand

2016-2019 Bachelor of Science in Chemical Engineering, Department of Chemical Technology, Faculty of Science, Chulalongkorn University, Bangkok, Thailand

HOME ADDRESS 174/86 Vibhavadi Rangsit 78, Sanam Bin, Don Mueang, Bangkok 10210

PUBLICATION

Proceeding:

1. Chaovarin, C., Yodpetch, V., Inkong, K., Kulprathipanja, S., and Rangsunvigit, P. (2022). Investigation of methane hydrate formation and dissociation in the presence of biofriendly amino acids for natural gas storage application. Proceedings of The 13th Research Symposium on Petrochemical and Material Technology and The 28th PPC Symposium on Petroleum, Petrochemicals, and Polymers, Bangkok, Thailand.

Presentation:

1. Chaovarin, C., Yodpetch, V., Inkong, K., Kulprathipanja, S., and Rangsunvigit, P. (2022). Investigation of methane hydrate formation and dissociation in the presence of biofriendly amino acids for natural gas storage application. Poster Presentation at The 13th Research Symposium on Petrochemical and Material Technology and The 28th PPC Symposium on Petroleum, Petrochemicals, and Polymers, Bangkok, Thailand.

2. Chaovarin, C., Inkong, K., Yodpetch, V., Kulprathipanja, S., and Rangsunvigit, P. (2022). Investigation of methane hydrate formation and dissociation in the presence of biofriendly amino acids for natural gas storage application. Poster Presentation at The 31st Thai Institute of Chemical Engineering and Applied Chemistry Conference.